RSC Advances

PAPER

View Article Online
View Journal | View Issue

Cite this: *RSC Adv.*, 2020, **10**, 23999

Fluorenone imidazolium salts as novel de Vries materials†

Korinna Bader,[a] Carsten Müller,[b] Yann Molard,[c] Angelika Baro,[a] Philipp Ehni,[a] Jakob Knelles[a] and Sabine Laschat *[a]

In ionic liquid crystals (ILCs) tilted mesophases such as SmC required for electro-optic devices are quite rare. We report a design concept that induced the SmC phase and enabled de Vries-like behaviour in ILCs. For this purpose, we synthesized and characterized a library of ILC derivatives **ImR(On,Ym)X** which consist of a rigid central fluorenone core containing an alkoxy or thioether side chain and connected *via* a flexible spacer to an imidazolium head group. The mesomorphic properties were studied by differential scanning calorimetry (DSC), polarizing optical microscopy (POM) and X-ray diffraction (XRD). Temperature-dependent measurements of smectic layer spacing d by small-angle X-ray scattering (SAXS) and of optical tilt angles by POM demonstrate that ILCs **ImR(On,Ym)X** undergo SmA–SmC phase transitions with maximum layer contraction values between 0.4% and 2.1%. The lowest reduction factor R of 0.2 at the reduced temperature $T - T_{AC} = -10$ K was calculated for **Im(O12,S14)Br**. Electron density calculations indicated a bilayer structure. Furthermore, temperature dependent emission studies show that self-assembling has a strong influence on the emission intensity of these ILCs.

Received 26th May 2020
Accepted 15th June 2020

DOI: 10.1039/d0ra04650g

rsc.li/rsc-advances

Introduction

Ionic liquid crystals (ILCs) combine the physical properties of ionic liquids with those of thermotropic liquid crystals[1–8] and thus provide highly desirable materials for anisotropically ordered 1D ion conductors in organic solar cells[9,10] and as solid electrolytes in lithium ion batteries.[11] While ILCs share many similarities with neutral thermotropic liquid crystals, they differ in the occurrence of certain mesophases.[1–8] The strong tendency of ILCs to nanosegregate ionic and non-charged segments during liquid crystalline self-assembly leads to a strong preference of the non-tilted SmA phase as their archetypal mesophase, while for example the tilted SmC phase is much less common among ILCs.[12–16] We have previously identified ILCs **1**, **2** showing rare SmC phases (Scheme 1), which consist of a calamitic core unit carrying one side chain and a flexible spacer connected to a cationic head group.[15–18] Upon examination of the order parameter of the SmA phase of these compounds it was found that the long range orientational order (S_2) in the SmA phase was much smaller as compared to the values obtained for SmA phases from non-ionic liquid crystals.[19–22] On the other hand, the 1D translational order (smectic order parameter ε) of the SmA phase of ILCs is much larger[17,18] as compared to non-ionic SmA phases.[23–26] Thus ILCs possess a high lamellar order but only a low long range orientational order as compared to neutral liquid crystals and in that respect behave similar to the so called de Vries materials.[26–29] De Vries materials have created much interest recently, because ferroelectric displays based on de Vries materials might overcome limitations of current nematic LC displays such as limited resolution and low optical efficiency.[30–47] One of the characteristic features of de Vries materials is their tilting transition without defect generation. These materials show no or only very low layer contraction upon the SmA to SmC phase transition, enabling ferroelectric displays without zig–zag defects caused by the chevron-like arrangement of the molecules in the mesophase. With regard to the design of calamitic liquid crystals displaying SmA and SmC phases and de Vries behaviour most previous work has focused on 5-phenylpyrimidines,[39,41,43,48–53] 2-phenylpyrimidines,[54–58] biphenyls,[40,44,59–64] thiadiazoles,[54,65] aroylhydrazones[66] and bent-core mesogens.[37,67–74] Lemieux and Ivanov have reported independently for non-charged liquid crystals **3–5** that a rigid fluorenone core promotes formation of the SmC phase.[75–80] As mentioned above, in contrast to neutral calamitic liquid crystals ILCs are rather reluctant to form SmC phases. Despite the few known examples,[12–18] it is still an ongoing challenge to develop design principles for ILCs displaying both SmA and SmC phases. Moreover, ILCs with de Vries properties should provide a general insight into the driving forces for layer contraction and layer tilting of ionic

[a]*Institut für Organische Chemie, Universität Stuttgart, Pfaffenwaldring 55, 70569 Stuttgart, Germany. E-mail: sabine.laschat@oc.uni-stuttgart.de*

[b]*Institut für Physikalische Chemie, Universität Stuttgart, Pfaffenwaldring 55, 70569 Stuttgart, Germany*

[c]*CNRS, ISCR-UMR 6226, ScanMAT-UMS 2001, University Rennes, 35000 Rennes, France. E-mail: yann.molard@univ-rennes1.fr*

† Electronic supplementary information (ESI) available. See DOI: 10.1039/d0ra04650g

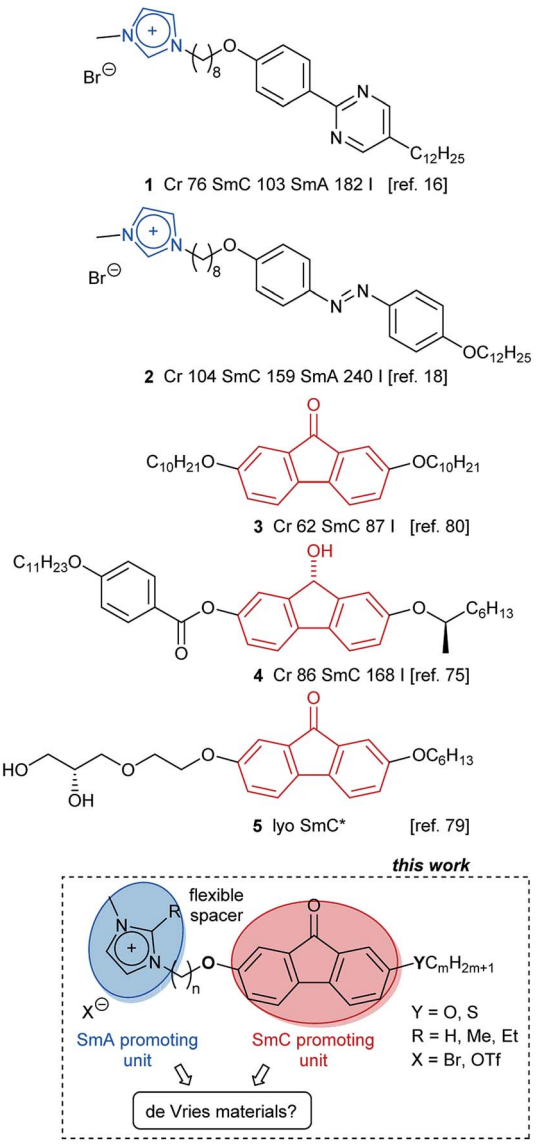

Scheme 1

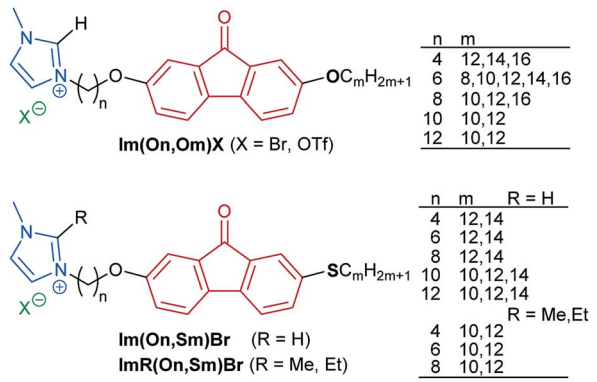

Scheme 2 Library of fluorenone ionic liquid crystals (ILCs).

mesogens and thus are relevant for electro-optic devices.[81] Thus, we were curious, whether combination of a SmA-promoting unit, such as an imidazolium head group with a SmC-promoting calamitic core, *i.e.* fluorenone, tethered together *via* a flexible alkyl spacer would eventually lead to ILCs displaying both SmA and SmC phases and a minimal layer contraction, *i.e.* de Vries-like behaviour. Our results reveal that such merging of concepts is indeed successful and provides ILCs with a very broad mesophase stability, unique de Vries behaviour and solid state luminescence. The results are discussed below.

Results and discussion

Synthesis of fluorenone imidazolium ILCs

In order to obtain structure–property relationships, a library of fluorenone ILCs **Im(On,Om)X** and **ImR(On,Sm)Br** was prepared (Scheme 2), where the following structural parameters were varied: alkoxy *vs.* thioether side chain with different chain lengths *m*, spacer lengths *n*, C-1 substituent R at the imidazolium head group and counterion. These target structures required a synthetic approach providing access to unsymmetrical fluorenones.

As shown in Scheme 3, the synthesis commenced with a sequential Suzuki cross coupling[82] of methyl 6-bromo-3-methoxybenzoate **6** with known borolanes **7a–f**[83–85] to give the biphenyl esters **8a–f**.

Subsequent saponification[86] provided biphenyl carboxylic acids **9a–f**, which were submitted to Friedel–Crafts acylation[87] *via* activation with thionyl chloride and reaction with $AlCl_3$ to give the fluorenones **10a–f**. For the selective deprotection of the methyl ether **10a–e** two protocols employing thiols were examined.

According to a method by Magano[88] *N*,*N*-diethyl-aminoethanethiol was deprotonated with NaO*t*Bu in DMF at room temperature and then treated with the respective fluorenone **10a–e** to give the hydroxyfluorenones **11a–e** in moderate yields (method A). Alternatively, dodecanethiol was used together with NaH in DMF at 80 °C (method B) following a procedure by Chae[89] resulting in higher yields of the desired hydroxyfluorenones **11b–e** with alkoxy side chains.

For the corresponding hydroxy fluorenones **13** with thioethers, a nucleophilic displacement of aryl fluoride by thionucleophiles as reported by Kaszyński[90] was planned as a key step. Upon treatment of **10f** with 2.0 equiv. of dodecanethiol and 1.3 equiv. of NaH in DMF at 80 °C,[90] the desired nucleophilic displacement competed with demethylation resulting in a mixture of 63% **12c** and 22% of **13c** (Scheme 3). This one-pot nucleophilic substitution/demethylation sequence could be optimized by employing equimolar amounts of thiol and NaH, *e.g.* giving 6% of **12c** and 82% of the target alcohol **13c**.

The hydroxyfluorenones were submitted to Williamson etherification with 1,ω-dibromoalkanes[91] to provide the corresponding ω-bromoalkoxyfluorenones **Br(On,Om)** and **Br(On,Sm)** in good yields, followed by reaction with the methylimidazoles **16a–c** (Scheme 3).[16] While the 2-*H*-substituted imidazolium salts **Im(On,Om)Br**, **Im(On,Sm)Br** could be isolated in pure form after chromatography through HBr-treated

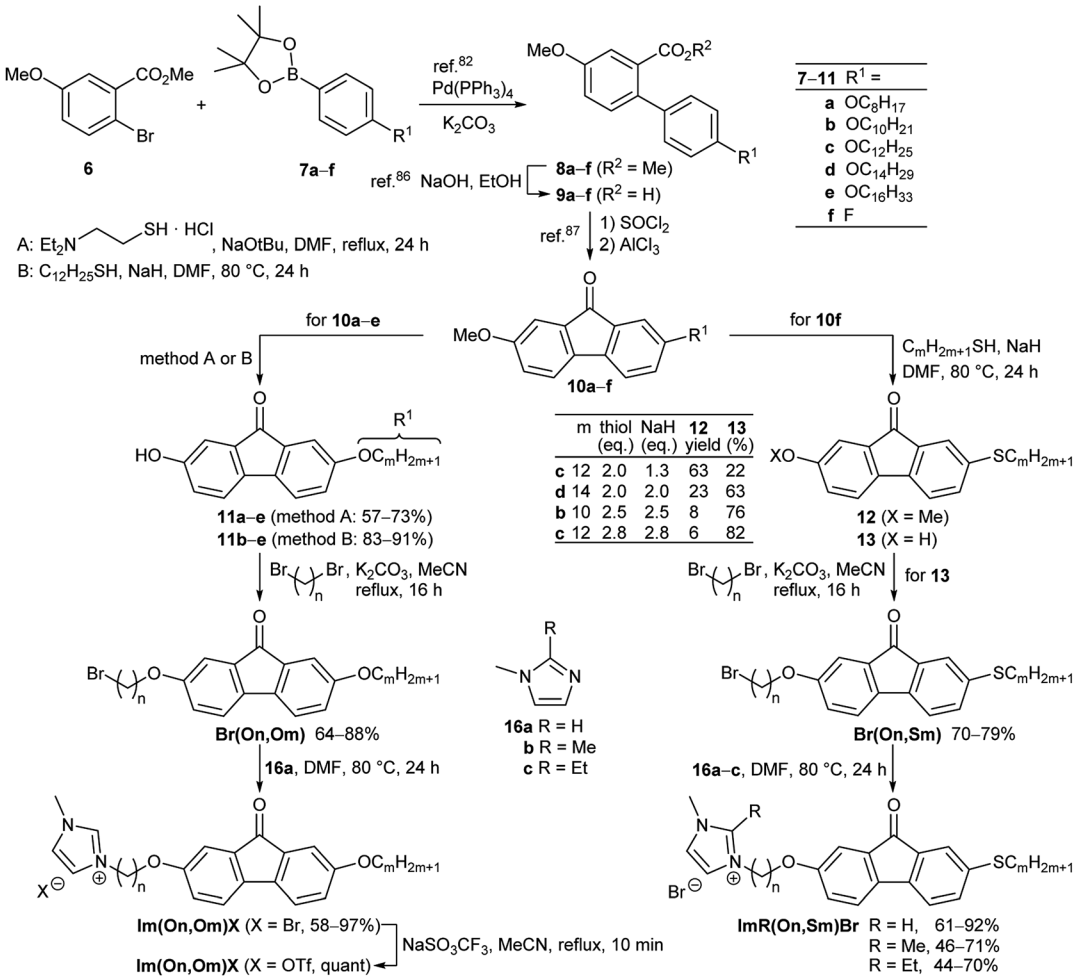

Scheme 3 Synthesis of the imidazolium salt ILCs Im(On,Om)X and ImR(On,Sm)Br.

silica, the corresponding 2-methyl- and 2-ethyl-substituted imidazolium bromides **ImR(On,Sm)Br** (R = Me, Et) required an additional recrystallization step, and thus lower overall yields were obtained. For a selected series **Im(On,Om)Br** the bromide counterion was replaced by triflate *via* salt metathesis[92] (Scheme 3).

Mesomorphic properties of the ω-bromoalkoxyfluorenones

First, the mesomorphic properties of the ILC precursors, *i.e.* the ω-bromoalkoxyfluorenones **Br(On,Ym)** were examined by differential scanning calorimetry (DSC), polarizing optical microscopy (POM) and X-ray diffraction (WAXS, SAXS). The DSC data are summarized in Fig. S1–S3, Tables S1 and S2 (see ESI†). Both linking atoms Y, side chain lengths *m* and spacer length *n* had a pronounced influence on the phase behaviour of **Br(On,Ym)**.

All ω-bromoalkoxyfluorenones **Br(On,Om)** showed enantiotropic mesomorphism. The DSC curves reveal supercooling for the mesophase-to-crystalline transition upon cooling from the isotropic liquid while clearing temperatures are maintained in heating/cooling scans. It should be noted that supercooling is quite common among ILCs[93–97] and was recently rationalized by cationic clustering.[98] Under the POM **Br(On,Om)** displayed focal-conic fan textures, which are characteristic of SmA phases (Fig. 1a, b and d). The broadest SmA phase in the series **Br(O6,Om)** with various chain lengths *m* was found for **Br(O6,O10)**. Upon variation of the spacer lengths *n* in the series **Br(On,O12)** the broadest mesophase widths of 21–22 K were detected for *n* = 8, 10. Thus both very short and very long spacers seem to disfavour lamellar mesophases. In contrast, only ω-bromoalkoxyfluorenones **Br(O6,S10)**, **Br(O8,S10)**, **Br(O8,S12)**, and **Br(O10,S14)** with a thioether side chain showed monotropic mesomorphism upon cooling. The clearing transitions ranged between 55 and 63 °C and melting temperature between 30–58 °C. The decreased clearing temperatures and resulting destabilization of the SmA phase by thioethers agree well with previous reports on calamitic phenylpyrimidines.[99,100] However, the increase of melting temperatures of **Br(On,Sm)** in comparison with **Br(On,Om)** is in contrast to these reports where thioethers led to lowering of melting points.

XRD experiments gave further insight into the phase geometry. The WAXS profile of an oriented sample of **Br(O6,O8)** showed a strong (001) layer reflection and a diffuse halo, which was tilted by 90° with respect to the (001) reflex, indicating an

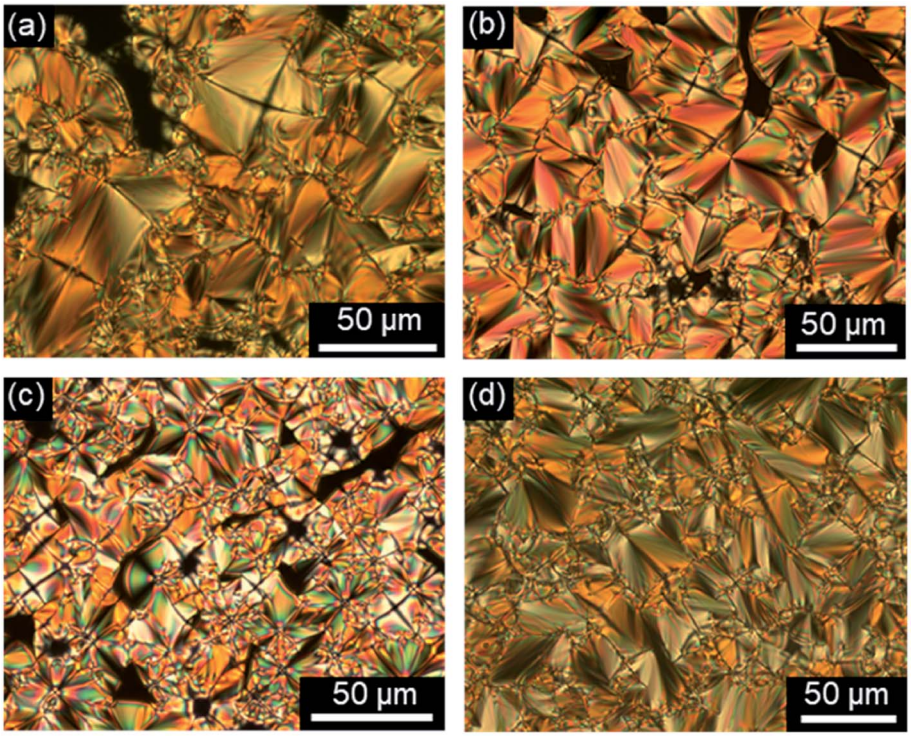

Fig. 1 Focal-conic fan textures as seen between crossed polarizers upon cooling from the isotropic liquid (cooling rate 5 K min^{-1}, magnification ×200). (a) **Br(O4,O12)** at 65 °C, (b) **Br(O6,O12)** at 71 °C, (c) **Br(O8,S12)** at 61 °C, and (d) **Br(O10,O12)** at 70 °C.

orthogonal SmA phase (Fig. 2a). In the SAXS profile a weak second order (002) reflection was visible besides the intense (001) reflection (Fig. 2b). From the (001) reflex the layer distance d was calculated according to equation $n\lambda = 2d \sin\theta$ and plotted against the temperature (Fig. S23, ESI†). Typical for SmA phases, layer distances d decreased with increasing temperature

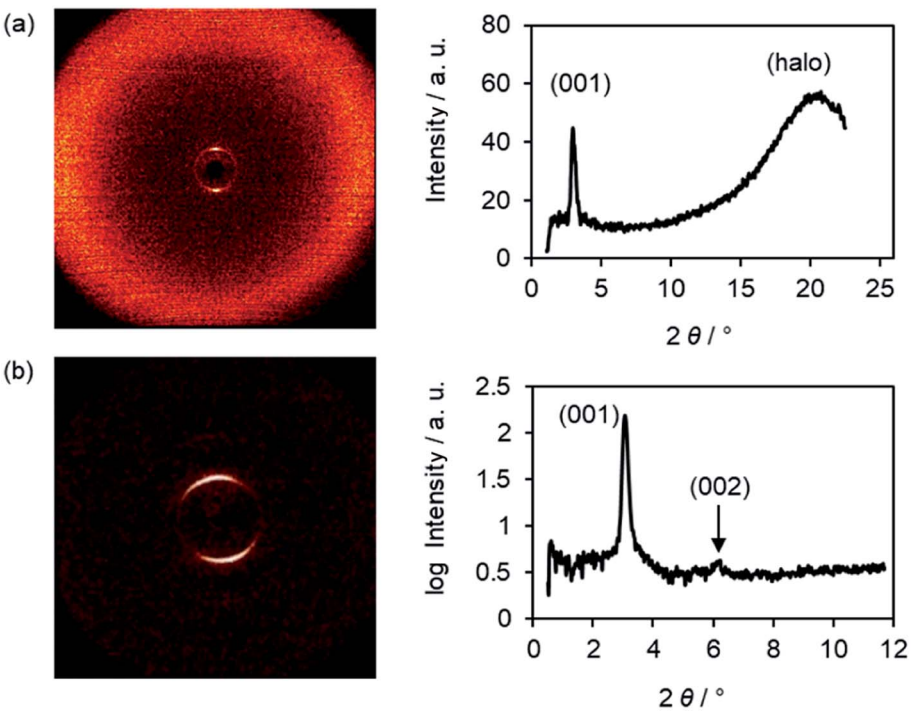

Fig. 2 (a) Wide-angle scattering (WAXS) and (b) small-angle scattering (SAXS) profile and the corresponding diffraction pattern of **Br(O6,O8)** at 45 °C.

due to decreased orientational order with increasing temperature. Furthermore, with increasing chain lengths the *d* values increased by 2.5 Å, which is equivalent to two CH_2 units. The exclusive formation of SmA phases of the ω-bromoalkoxyfluorenones **Br(On,Ym)** can be rationalized by the presence of SmA-promoting halogens as suggested by Giesselmann and Lemieux,[101] *i.e.* reduced electrostatic repulsion between alkyl chains and improved van der Waals interaction between the aryl units rather than polar interactions at the interfaces between the smectic layers as was proposed by Goodby.[102]

Mesomorphic properties of the fluorenone ILCs

Phase transition temperatures and enthalpies of fluorenone ILCs **Im(On,Om)X** were determined by DSC from the first heating scans (Table S3 and Fig. S4, ESI†). Due to thermal decomposition of the samples caused by high isotropization temperatures in subsequent heating/cooling cycles no further transitions were detectable. In most cases SmC–SmA phase transitions were undetectable by DSC but were visible under the POM. Only in a few cases weak first order transitions with very small enthalpy changes were detected by DSC, which is in good agreement with previous work (Fig. S13–S17, ESI†).[53,103] As exemplified for **Im(O6,Om)Br** in Fig. 3, the melting points remained relatively constant at 72–84 °C, while the clearing points were much stronger affected by the alkyl chain lengths *m* and increased from 237 °C for **Im(O6,O8)Br** up to 273 °C for **Im(O6,O16)Br** resulting in the broadest mesophase (192 K) for **Im(O6,O16)Br**. All ILCs within this series showed small SmC phases (10–32 K) and relatively broad SmA phases (149–164 K).

In contrast, **Im(O12,Om)Br** (m = 10,12) with a long C12 spacer showed no evidence for decomposition and thus DSC curves of three heating/cooling cycles were fully reproducible (Fig. S4, ESI†). The small transition enthalpies of 0.5–0.6 kJ mol^{-1} are typical for SmC–SmA transitions.[18]

As shown for **Im(On,O12)Br** with increasing spacer lengths *n* clearing temperatures decreased considerably (Fig. 3), which can be rationalized by the increased flexibility of the ILC molecules with larger spacers resulting in a decreased lamellar order. This trend is in agreement with previous observations on azobenzene ILCs.[17] It should be noted that the behaviour of ILCs consisting of cationic group–spacer–mesogenic core–side chain is more complex as compared to ILCs containing side chain–cationic group–side chain.

Melting temperatures changed only little (68–90 °C), however, the stability of the SmC phase was strongly affected by variation of the spacer lengths *n*. While **Im(O4,O12)Br** showed only a monotropic SmA phase, derivatives with $n > 4$ displayed also enantiotropic SmC phases under the POM. Furthermore, the stability increased with increasing spacer lengths *n*, resulting in the broadest SmC phase (53 K) for $n = 10, 12$, while SmC phase widths of 21–22 K were found for derivatives with $n = 6, 8$ (Fig. 3).

Various experimental studies from the literature[20,104] including very recent theoretical work by Saielli[105] described a strong influence of the counterion on transition temperatures and mesophase type. Therefore, we surmised that an exchange of the counterion might be helpful to overcome the thermal decomposition. However, the triflate counterion decreased the clearing temperature significantly to 114–130 °C only for **Im(O6,O8)OTf** and **Im(O8,O10)OTf**. The triflate was stable and the complete phase sequence was reproducible over three heating/cooling cycles (Fig. S5, ESI†). ILCs **Im(On,O14)OTf** (n = 4, 6) showed only a slight decrease of the clearing temperature and thus isotropization was still accompanied by thermal decomposition. Most importantly, the triflate counterion affected the mesophase type, resulting in loss of the SmC phase. Similar results were reported by Trbojevic for guanidinium ILCs connected *via* a flexible alkyl spacer to a rod-like biphenyl unit,[15] where replacement of chloride by triflate decreased the clearing transition but suppressed the SmC phase in favor of the SmA phase.

The phase behaviour of fluorenone imidazolium bromides **Im(On,Sm)Br** carrying thioether side chains was similar to that

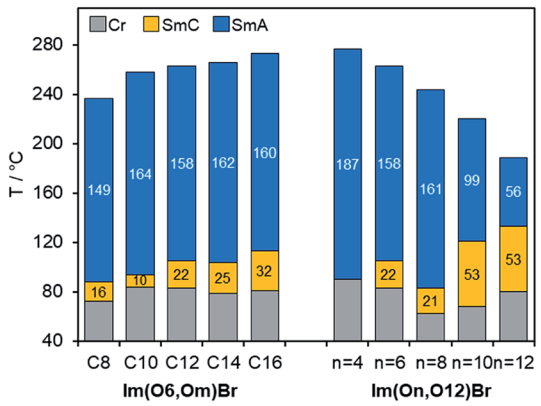

Fig. 3 Mesophase stabilities of Im(O6,Om)Br and Im(On,O12)Br with varying alkoxy side chain *m* and varying spacer lengths *n*, respectively. The values in the bar diagram correspond to the mesophase temperature ranges. Phase transitions were determined by DSC (1st heating) and POM (SmA–SmC transition). Im(O12,O12)Br (3rd heating).

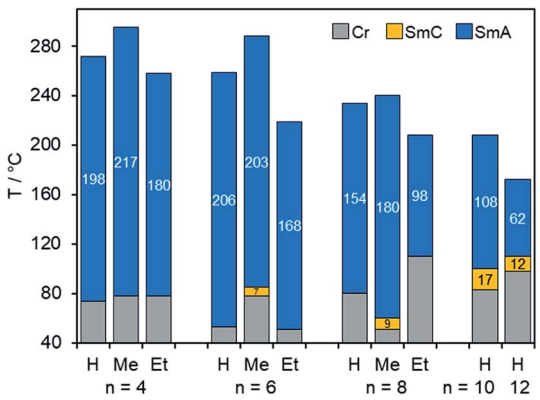

Fig. 4 Comparison of mesophase stabilities of ILCs ImR(On,S12)Br with variable spacer lengths *n* upon heating. The values in the bar diagram correspond to the mesophase temperature ranges. Phase transitions were determined by DSC (1st heating) and POM (SmA–SmC transition), for Im(On,S12)Br (n = 10, 12) 3rd heating (see Tables S4 and S5, ESI†).

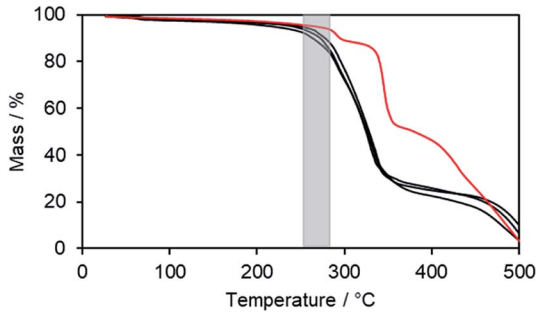

Fig. 5 TGA thermograms of imidazolium bromides Im(On,O14)Br (n = 4,6), Im(O8,O16)Br (black lines) and triflate Im(O4,O14)OTf (red line). The grey zone illustrates the clearing temperature range.

of the corresponding **Im(On,Om)Br**. As shown for **Im(On,S12)Br** with dodecylthio side chain, clearing temperatures decreased with increasing spacer lengths n (R = H, Fig. 4). Thioethers **Im(On,S12)Br** with short spacers n = 4, 6, 8 formed only SmA phases with broad phase widths of 154–206 K, whereas the homologous ILCs with longer spacers (n = 10, 12) displayed additional SmC phases. However, the phase stability was not increased by longer spacers. The replacement of oxygen with sulfur resulted in a significant destabilization of the SmC phase, and the phase ranges decreased to 12–17 K as compared to the corresponding ILCs **Im(On,O12)Br** (53 K).

The influence of substituent R at C-1 of the imidazolium head group on the mesophase stability of ILCs **ImR(On,S12)Br** is also shown in Fig. 4. Bromides **ImR(On,S12)Br** displayed broad SmA phases with phase widths ranging from 62–217 K. Within this series only the ILCs with H- or methyl-substituted imidazolium head group **ImH(On,S12)Br** and **ImMe(On,S12)Br** formed enantiotropic SmC phases with minimum spacer lengths of n = 10 (for R = H) and n = 6 (for R = Me). The corresponding ILCs **ImEt(On,S12)Br** showed only monotropic SmC phases under the POM upon cooling (Fig. 7 and S18–S20, ESI†). The clearing points were affected by substituent R. For example, for **ImR(O4,S12)Br** with a short C4 spacer the clearing point increased from 272 °C (R = H) to 295 °C (R = Me) and decreased to 258 °C (R = Et). It should be noted that ethyl-substituted imidazolium ILCs were still prone to thermal decomposition. These results are in good agreement with previous work by Swager,[106] Butschies[92] and Kapernaum.[17]

To obtain further information on the thermal stability, ILCs **Im(On,O14)Br** (n = 4, 6) and **Im(O8,O16)Br** with clearing transitions >270 °C were submitted to thermogravimetric analysis (TGA) (Fig. 5). The ILCs were stable up to 200 °C (black curves). Upon further heating thermal decomposition was accompanied by loss of mass. The clearing points (grey zone) are located above the decomposition temperatures. As compared to the bromides, imidazolium triflate **Im(O4,O14)OTf** showed a slightly improved thermal stability (red curve), however, the clearing point (243 °C) is still within the decomposition range. Thus, TGA experiments confirmed the DSC results. Presumably the triflate anion is less nucleophilic than bromide and does not cause thermally induced dealkylations of the imidazolium unit. When comparing the DSC results of **Im(On,Om)Br** with **Im(On,Om)OTf** (Table S3, ESI†), it is remarkable that for imidazolium salts with large length differences between spacer n and side chain m, the clearing temperature decreased by ~50 K, whereas the clearing temperature of imidazolium salts with similar lengths n, m decreased by >100 K.

Investigations of fluorenone imidazolium bromides **Im(On,Om)Br** with alkoxy side chains under the POM showed large areas of homeotropic alignment. Birefringent areas could only be observed at phase boundaries and air bubbles (Fig. S13–S17, ESI†). ILCs **Im(O4,Om)Br** only showed fan textures (Fig. S13, ESI†), while imidazolium bromides forming SmA and SmC phases displayed both fan textures characteristic of SmA and at lower temperatures broken fan and Schlieren textures typical for SmC phases,[107] as shown in Fig. 6 for **Im(O10,O12)Br**.

The POM studies provided initial hints for de Vries-like behaviour. The color change of the fan (SmA)/broken fan (SmC) texture of **Im(O10,O12)Br** during SmA–SmC phase transition from orange brown to pale blue indicated an increase in birefringence in the SmC phase and thus an increased orientational order, which is reported to be characteristic for de Vries-like materials.[30,54,55,65,103,108]

Fluorenone imidazolium bromides **ImR(On,Sm)Br** with thioether side chains formed fan and Bâtonnet textures or large

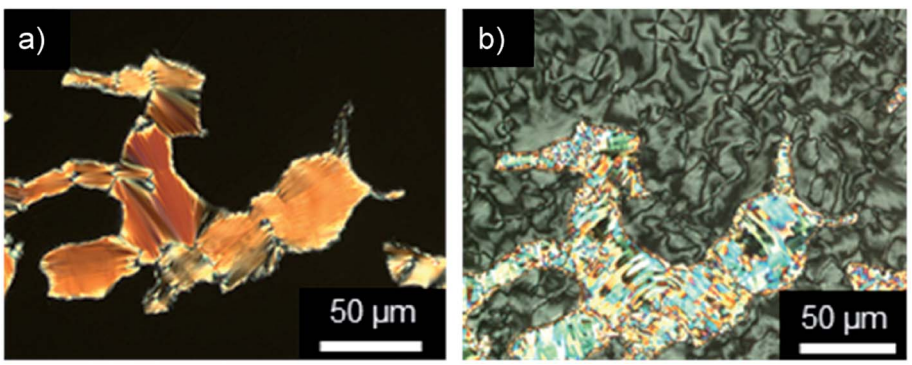

Fig. 6 Textures of Im(O10,O12)Br as seen between crossed polarizers at (a) 132 °C and (b) 121 °C upon cooling from the isotropic liquid (cooling rate 5 K min^{-1}, magnification ×200).

homeotropic areas in the SmA phase and at lower temperatures Schlieren textures typical for SmC phases under the POM (Fig. 7). While for ILCs **ImR(On,Sm)Br** with R = H Schlieren textures occurred at a minimum spacer length $n = 8$ and side chain length $m = 14$, for the corresponding ILCs **ImMe(On,Sm)Br** and **ImEt(On,Sm)Br** Schlieren textures appeared already for spacer lengths $n = 6$.

The strong tendency of the ILCs for homeotropic alignment in the SmA phase could be suppressed by using nylon-coated glass cells (1.6 μm). For example, upon cooling from the isotropic liquid ILCs **Im(O10,Y10)Br** displayed well-developed fan textures (Fig. 8a and c), which transformed into broken fan textures upon further cooling (Fig. 8b and d).

As expected from temperature-dependent SAXS experiments, layer distances d in the SmA phase of **Im(On,Om)X** and **ImR(On,Sm)Br** decreased with increasing temperature (Fig. S23 and S24, ESI†). The experimentally determined layer distances d were almost twice as large as compared to the calculated molecular lengths L_{calc} (molecular mechanics, force field: MMFF94s; software Avogadro[109]) of an all-trans fully extended conformation. The ratios d/L_{calc} were approximately 1.7–1.8 suggesting the presence of partially interdigitated smectic bilayers, that are also very prominent in de Vries-like materials (Tables S7 and S8, ESI†).

Investigation of de Vries-like properties of the fluorenone ILCs

In the WAXS pattern of the SmA phase of **Im(O12,O10)Br** at 169 °C three sharp reflexes in the small angle region and a diffuse maximum (halo) in the wide angle section are visible (Fig. 9a). The XRD pattern remained similar during SmA–SmC

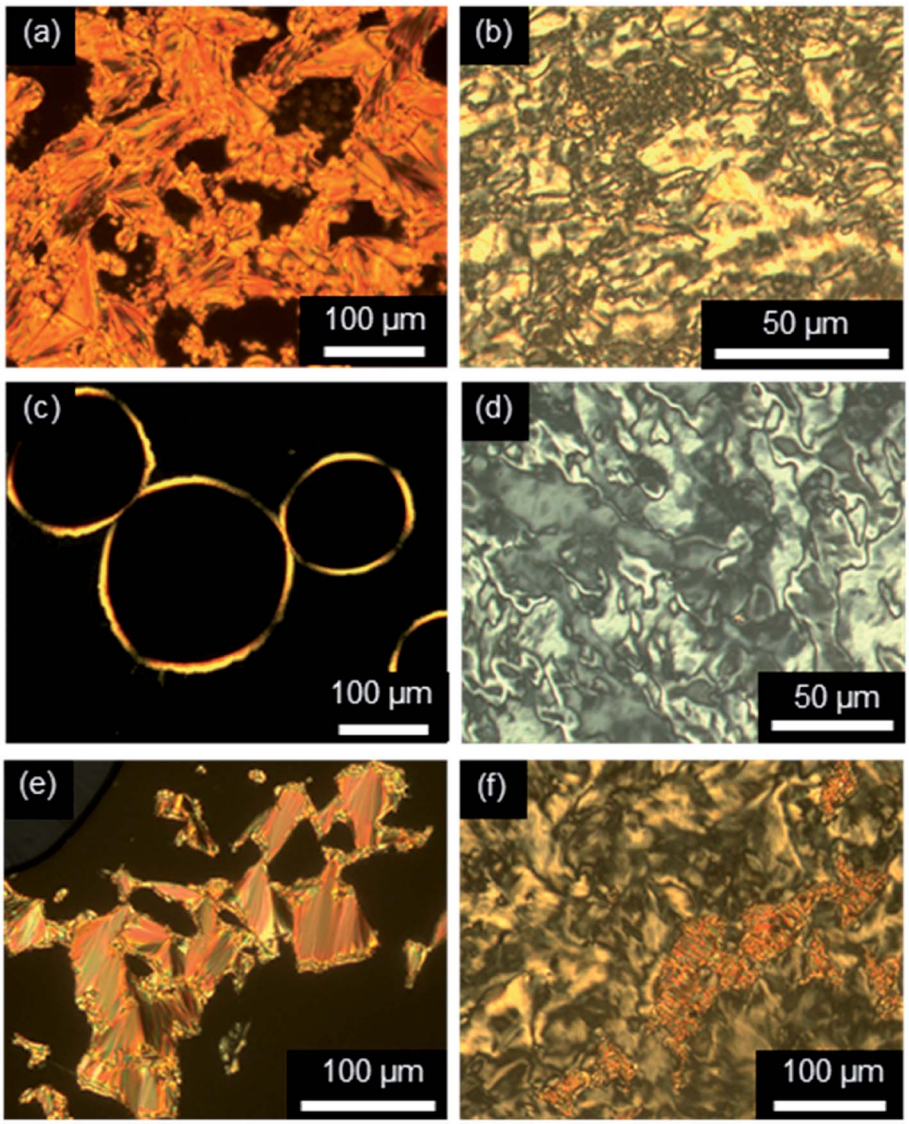

Fig. 7 Textures as seen between crossed polarizers upon cooling from the isotropic liquid. (a and b) **ImMe(O6,S12)Br** at 180 °C and 52 °C, (c and d) **ImEt(O8,S12)Br** at 158 °C and 69 °C, and (e and f) **ImH(O10,S12)Br** at 128 °C and 94 °C, (cooling rate 5 K min^{-1}, magnification ×100 (a, c and e), magnification ×200 (b and d)).

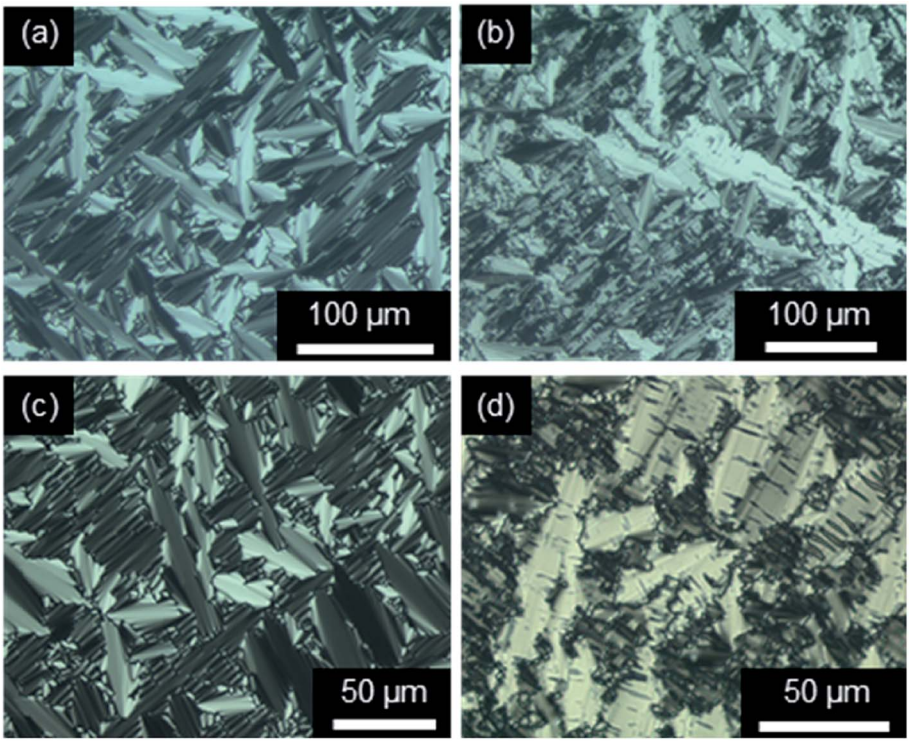

Fig. 8 Textures of (a and b) **Im(O10,O10)Br** at 175 °C and 120 °C (magnification ×100) and (c and d) **Im(O10,S10)Br** at 180 °C and 86 °C (magnification ×200) under POM in a nylon-coated glass cell of 1.6 μm thickness (cooling rate 10 K min^{-1}).

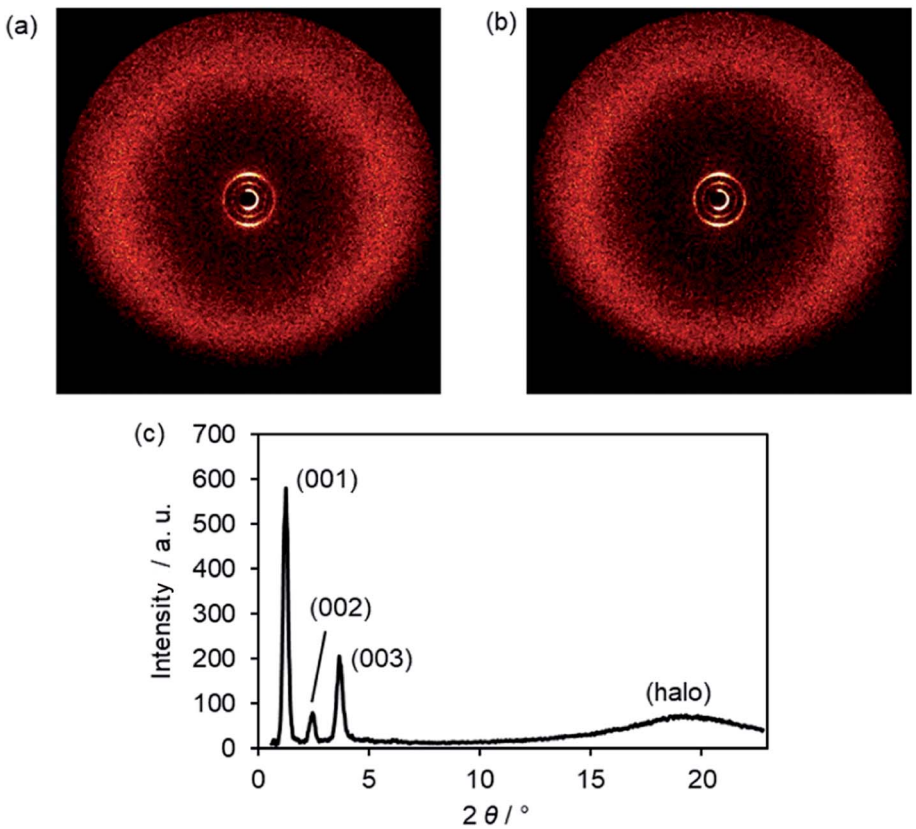

Fig. 9 (a) WAXS diffraction image of **Im(O12,O10)Br** at 169 °C in the SmA phase, (b) WAXS diffraction image and (c) the corresponding scattering profile of **Im(O12,O10)Br** at 83 °C in the SmC phase.

transition (Fig. 9b), because ILCs **ImR(On,Ym)X** did not give oriented samples.[17,18]

High order layer reflections up to 4th order (004) could be observed for ILCs **ImR(On,Ym)X** (Table S8, ESI†), suggesting that the smectic phases of the ILCs possess a high degree of translational order presumably due to the strong nano-segregating effect of the ionic head group.[21,30,110]

One parameter for de Vries-like behaviour is the maximum layer contraction at the SmA–SmC phase transition. Therefore, the smectic layer spacing d of ILCs **ImR(On,Ym)Br** as a function of temperature was measured by small-angle X-ray scattering (SAXS). The layer distances d were calculated from the (001) reflex at different temperatures, where d_{AC} denotes the layer distance at the SmA–SmC transition temperature T_{AC}. At the temperature where the largest layer shrinkage occurred, the maximum layer contraction S_{max} was determined.

The profiles of normalized layer spacings d/d_{AC} *vs.* reduced temperature $T - T_{AC}$ for ILCs **Im(On,Om)Br** with an alkoxy side chain are summarized in Fig. 10 and Table 1. Estimated standard deviations were <5%. The temperature-dependent d/d_{AC} curves are similar in this series. Upon cooling an expansion in the SmA phase until the transition temperature was observed. At transition into the SmC phase, the layer spacing initially decreased and then increased upon further cooling. This behaviour is typical for de Vries-like materials, while in conventional liquid crystals the layer thickness decreases continuously in the SmC phase resulting in larger layer contractions.[50] As seen in Fig. 10a, the maximum layer contraction S_{max} decreases with the length m of the alkoxy side chain, from 2.1% for **Im(O6,O8)Br** to 0.5% for **Im(O6,O16)Br** (Table 1).

A similar trend was observed for **Im(O10,Om)Br** and **Im(O12,Om)Br** (Fig. 10c and d). However, in the series of **Im(O8,Om)Br** the trend was less clearcut. ILC **Im(O8,O16)Br** exhibited a maximum layer contraction $S_{max} = 0.7\%$, but **Im(O8,Om)Br** with $m = 10$, 12 gave similar S_{max} values of 1.5% and 1.4% (Fig. 10b and Table 1).

According to the d/d_{AC} *vs.* $T - T_{AC}$ profiles, ILCs **Im(On,Sm)Br** with thioether side behaved similarly, *i.e.* the maximum layer contractions decrease with increasing side chain length m (Fig. 11a, b and Table 1). In contrast, the maximum layer contraction of the ILCs **ImMe(On,Sm)Br** and **ImEt(On,Sm)Br** with methyl or ethyl substituents at the imidazolium unit (R = Me, Et) did not show any clear trend (Fig. 11c, d and Table 1).

The alkyl chain lengths effect on the layer contraction might be rationalized by the interdigitation with longer chains showing a higher degree of interdigitation as compared to shorter chains in agreement with recent studies by Wöhrle on

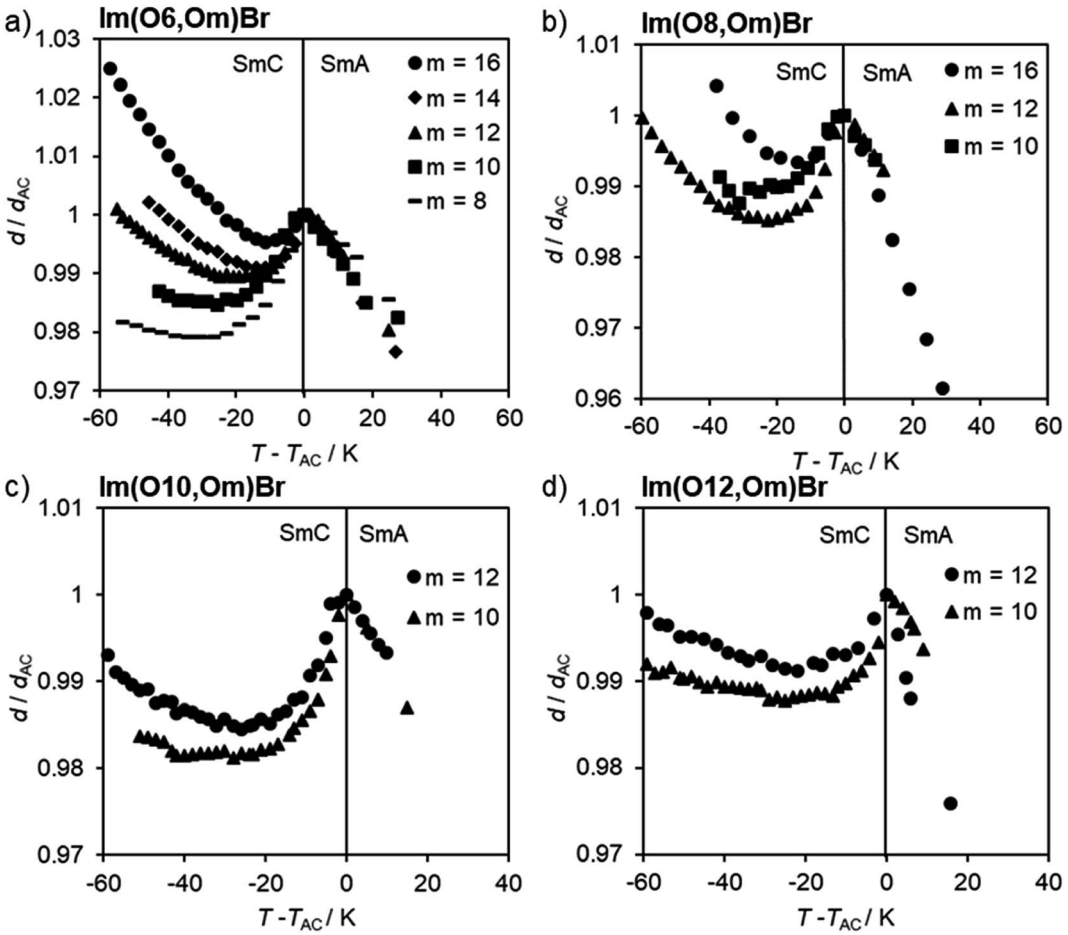

Fig. 10 Layer spacing d/d_{AC} *vs.* reduced temperature $T - T_{AC}$ profiles of Im(On,Om)Br.

Table 1 Maximum layer contraction S_{max}, calculated from the layer spacing d_{AC} at the SmA–SmC transition and the layer spacing d_C in the SmC phase of ILCs **ImR(On,Ym)Br** at the reduced temperature $T - T_{AC}$

Compound	$T - T_{AC}$/K	d_{AC}/Å	d_C/Å	S_{max}/%
Im(O6,O8)Br	−30	57.7	56.5	2.1
Im(O6,O10)Br	−26	63.8	62.8	1.5
Im(O6,O12)Br	−19	63.7	63.1	1.1
Im(O6,O14)Br	−14	69.9	69.3	0.9
Im(O6,O16)Br	−11	70.3	70.0	0.5
Im(O8,O10)Br	−31	66.0	65.2	1.4
Im(O8,O12)Br	−23	66.3	65.3	1.5
Im(O8,O16)Br	−14	74.1	73.6	0.7
Im(O10,O10)Br	−28	64.7	63.4	1.9
Im(O10,O12)Br	−26	68.0	67.0	1.5
Im(O12,O10)Br	−25	66.7	65.9	1.2
Im(O12,O12)Br	−22	72.0	71.4	0.9
Im(O8,S14)Br	−10	72.9	72.6	0.4
Im(O10,S10)Br	−13	68.9	68.1	1.1
Im(O10,S12)Br	−14	72.1	71.4	0.9
Im(O10,S14)Br	−6	72.8	72.4	0.5
Im(O12,S10)Br	−25	71.1	70.4	1.0
Im(O12,S12)Br	−6	74.5	73.8	0.9
Im(O12,S14)Br	−10	76.8	76.5	0.4
ImMe(O6,S12)Br	−17	69.4	68.8	0.9
ImMe(O6,S14)Br	−11	71.1	70.6	0.7
ImMe(O8,S12)Br	−20	70.7	70.0	1.0
ImMe(O8,S14)Br	−19	71.9	71.2	1.1
ImEt(O6,S12)Br	−14	66.5	65.7	1.1
ImEt(O8,S10)Br	−11	67.3	66.5	1.2
ImEt(O8,S12)Br	−17	70.7	69.8	1.4

SmA phases of MIDA boronates.[111] The determined d/L_{calc} ratios, however, did not show a clear trend (Tables S7 and S8, ESI†). For example, the **Im(O6,Om)Br** series revealed d_{AC}/L_{calc} ratios at the SmA–SmC phase transition of 1.79 ($m = 8$), 1.84 ($m = 10$), 1.71 ($m = 12$), 1.76 ($m = 14$), and 1.67 ($m = 16$). The pronounced color change of the textures observed for **ImR(On,Ym)Br** by POM during SmA–SmC transition indicated an increase in birefringence, which correlates with an increase in orientational order parameter S_2.[45–47,53] Therefore, we assume that the orientational order increased in the SmC phase and compensation for a large portion of the maximum layer contraction. However, due to unavailability of oriented samples of fluorenone ILCs **ImR(On,Ym)Br** for XRD studies we failed to clarify which effect compensates layer shrinkage and is responsible for the de Vries-like properties.

An alternative method to rationalize the beneficial influence of the alkyl chain lengths on the layer contraction is the so-called zig–zag model, originally proposed by Bartolino, Doucet and Durand,[112] and later confirmed by Böffel[113] and Clark.[114] In the zig–zag model the rigid cores are tilted to larger extent than the aliphatic chains in the SmC phase, *i.e.* the tilt of the layers is mainly caused by the tilted orientation of the rigid aromatic cores rather than the alkyl chains (Fig. 12).

The zig–zag model has also been implemented in the Boulder model by Walba and Clark to explain the polarization of ferroelectric liquid crystals.[115–117] According to this model an increase of the non-tilted alkyl chains should lead to a smaller layer contraction at the SmA–SmC phase transition.

The de Vries-like behaviour can be quantified by the reduction factor R, which considers both maximum layer contraction and optical tilt angle θ_{opt} in the SmC phase measured as a function of temperature by POM.[18,53,55,65,103] As the samples were filled in ITO glass cells with rubbed nylon alignment layer (1.6 μm thickness) by isotropic heating, only those ILCs could be investigated, which were thermally stable above the isotropization temperature based on their reproducible DSC curves. As an example, planar textures of **Im(O12,O10)Br** are shown in Fig. 13. In the SmA phase uniform domains are visible due to a parallel orientation of the director n with respect to the layer normal k (Fig. 13a), while in the SmC phase two different domain structures with different brightness are visible (Fig. 13b and c).

Optical tilt angles θ_{opt} were measured by POM as function of reduced temperature $T - T_{AC}$ in the absence of an electrical field upon cooling. In the SmA phase the director n is parallel to the layer normal k and thus $\theta_{opt} = 0$ (Fig. 14).

At $T - T_{AC} = 0$, the optical tilt angle θ_{opt} of the SmC phase increased significantly and then steadily increased upon further cooling. The abrupt increase of θ_{opt} indicates a 1st order SmA–SmC transition. This is in accordance with the DSC measurements, where for several compounds small peaks at the transitions from SmA to SmC were observed. In the series of ILCs with alkoxy side chain **Im(On,Om)Br** θ_{opt} increased up to 36° (Fig. 14a). The optical tilt angle profile of ILCs with thioether side chain **Im(On,Sm)Br** reveals slightly lower optical tilt angles (28–32°) (Fig. 14b). No general trend regarding spacer lengths n or alkyl chain lengths m could be detected.

From the maximum layer contraction and the optical tilt angle θ_{opt} the reduction factor R was calculated according to equation $R = \delta(T)/\theta_{opt}(T) = \cos^{-1}[d_C(T)/d_{AC}]/\theta_{opt}(T)$ for a given temperature.[53,118] The R values, maximum layer contraction S_{max} and optical tilt angle θ_{opt} at the reduced temperature $T - T_{AC}$ are summarized in Table 2.

The ILCs have R values ranging from 0.20 to 0.41 indicating a high de Vries-like behaviour. Thus, our design concept not only induced the rare SmC phase but also enabled de Vries behaviour with layer contractions S_{max} and R values, which are comparable to those of known neutral liquid crystalline de Vries materials[50,53,65] and further extends the scaffolds of ILCs previously developed by Kapernaum.[17,18] Moreover, it confirms that fluorenones are beneficial for de Vries ILCs. In agreement with the procedure reported by Lemieux[103] the $\theta_{opt}(T)$ profiles were fitted to the power law,[103] which provided the order parameter β related to the SmA–SmC transition (see also ref. 24 in Lemieux[103]). The ILCs possessed β values of 0.19–0.24, *i.e.* indicating weak 1st order transitions or tricritical point transitions (in case of $\beta = 0.25$) in agreement with Lemieux' observations (for details see Fig. S25, ESI†).

Calculation of the electron density

Based on layer reflections from SAXS experiments the electron density distribution in the smectic phase was obtained. The

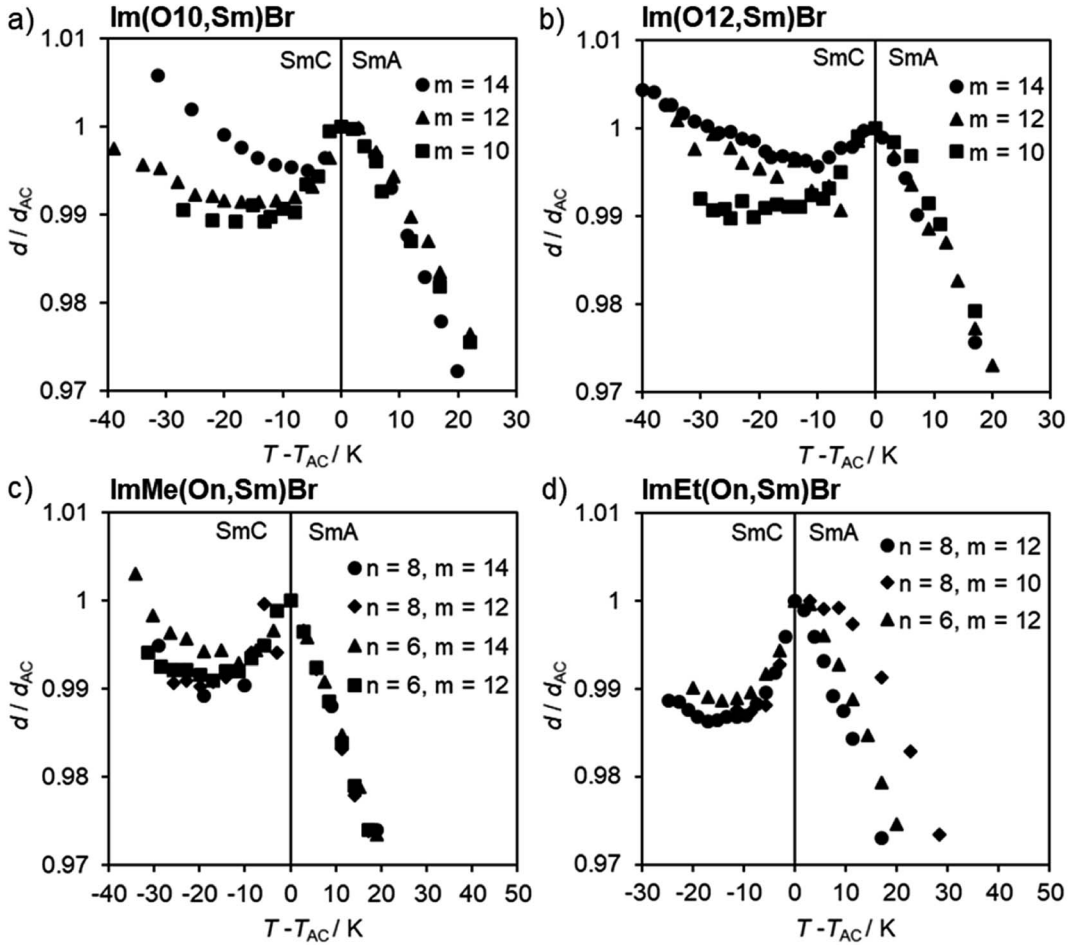

Fig. 11 Layer spacing d/d_{AC} *vs.* reduced temperature $T - T_{AC}$ profiles of **ImR(On,Sm)Br** with R = H (a and b), Me (c), Et (d).

electron density profile $\rho(z)$ along the director n was calculated by using eqn (1).[119]

$$\rho(z) = \sum_{l=1}^{m} a_l \cos\left(\frac{l2\pi z}{d_{00l}}\right) \quad (1)$$

From the intensity of the Bragg reflections (00l) and subsequent correction *via* the Lorentz factor[120] the square values $|a_l|^2$ were determined, while the signs of the a_l coefficients remained indefinite.[121] Therefore, all possible combinations of signs of the different a_l coefficients must be generated and submitted to a plausibility check. The imidazolium bromides **Im(On,Ym)Br** showed three layer reflections and therefore three coefficients a_1, a_2 and a_3 could be determined. The results are summarized in Table 3.

The electron density profile and the packing model of **Im(O12,O10)Br** are shown in Fig. 15. A large maximum of the electron density $\rho(z)$ is visible in the region of the ionic head groups, forming a charged sublayer. In the region of the aliphatic spacer a local minimum of the electron density $\rho(z)$ is visible and a local maximum due to the aromatic fluorenone core. Along the terminal alkoxy side chains, the electron density $\rho(z)$ shows a global minimum. For the other fluorenones in Table 3 analogous density profiles were obtained (Fig. S26, ESI†).

Absorption and emission properties of fluorenone precursors and ILCs

UV/vis data of imidazolium salts **Im(On,Ym)X** and their precursors are shown in Fig. 16. All fluorenone derivatives with an alkoxy side chain displayed absorption maxima at λ_{max} = 272–274 nm with a shoulder at lower wavelengths and two smaller bands at 302 nm and 314 nm, respectively (Fig. 16a).[122] The intense bands at 272–274 nm were assigned to the π–π* transition of the fluorenone core.[123,124] The UV/vis spectra were neither affected by different donor groups at the fluorenone core, *i.e.* methoxy, alkoxy or hydroxy nor different anions (bromide *vs.* triflate). However, the replacement of alkoxy by thioether side chains resulted in a bathochromic shift of the absorption maxima to λ_{max} = 282–283 nm (Fig. 16b).

This effect has been used for organic solar cells and field effect transistors to decrease the HOMO–LUMO gap and to improve the charge carrier mobility.[125] In contrast, the strongly electron-withdrawing fluoro substituent in **10f** shifted the absorption maximum hypsochromically to λ_{max} = 267 nm (Fig. S27†). All studied fluorenones were orange-red amorphous

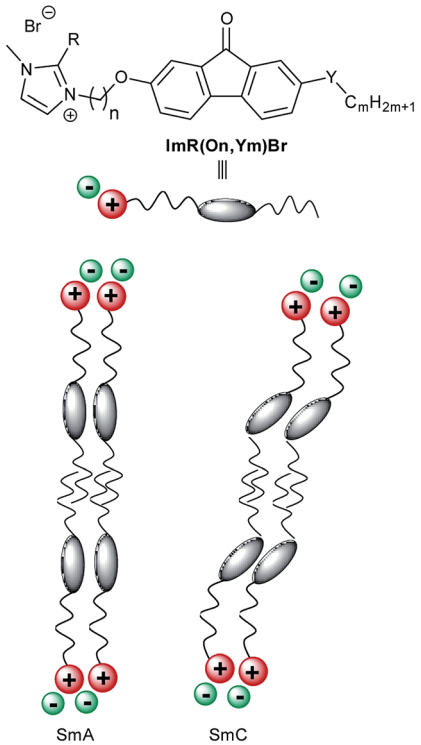

Fig. 12 Schematic illustration of the SmA and SmC phase of ILCs ImR(On,Ym)Br.

solids due to a low absorption in the visible region. A weak band around 400 nm was assigned to symmetry-forbidden n–π* transition of the carbonyl group (Fig. 16, inset).[123,124]

For potential applications bulk emission properties are particularly interesting. Therefore, selected samples were studied by solid state fluorescence spectroscopy utilizing a polarizing optical microscope equipped with UV light source (λ_{exc} = 350–380 nm) and photodetector. The method is limited to thermally stable compounds, because the samples required isotropization and thermal annealing to obtain uniform thin films for solid state emission spectra. The solid state emission spectra of **Br(O6,O16)**, exemplified in Fig. 17a, displayed at 25 °C a strong band at λ_{em} = 604 nm with two shoulders at longer wavelengths caused by the excimer emission due to fluorenone–fluorenone interactions.[122] At higher temperatures the intensity of the shoulder at longer wavelengths (635 nm) resulting from vibronic coupling increased.

The emission intensity was measured as a function of temperature upon cooling from the isotropic liquid (Fig. 17c). In the isotropic liquid the emission intensity was only 30% of the intensity at 25 °C (I_{25}). The I_{80}/I_{25} value decreased to 0.2 (20%) in the SmA phase and remained constant throughout the whole temperature range of the phase. Upon transition into the crystalline phase at 35 °C a strong increase of the emission was visible. It should be noted, that the SmA–Cr transition was detected at 51 °C by DSC (dashed line in Fig. 17c). The different emission intensities could also be observed *via* the POM pictures under irradiation with UV light (Fig. 17e).

A different behaviour of the bulk emission was observed for fluorenone **Br(O8,S12)** with thioether side chain (Fig. 17b, d and f). A strong emission at λ_{em} = 600 nm was observed in the isotropic liquid. Upon cooling and at the I–SmA transition the

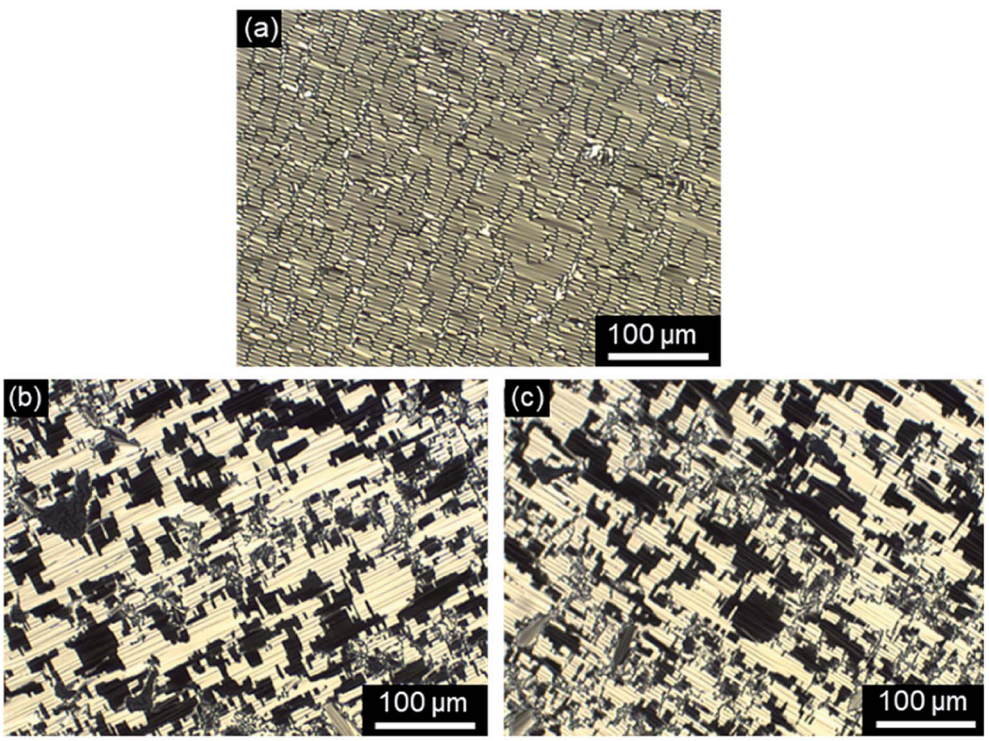

Fig. 13 Textures of **Im(O12,O10)Br** observed under the POM in a glass cell with rubbed nylon alignment layer of 1.6 μm thickness upon slow cooling from the isotropic liquid to achieve planar alignment. (a) At 160 °C in the SmA phase, and (b and c) at 135 °C in the SmC phase (cooling rate 0.2 K min^{-1}, magnification ×200).

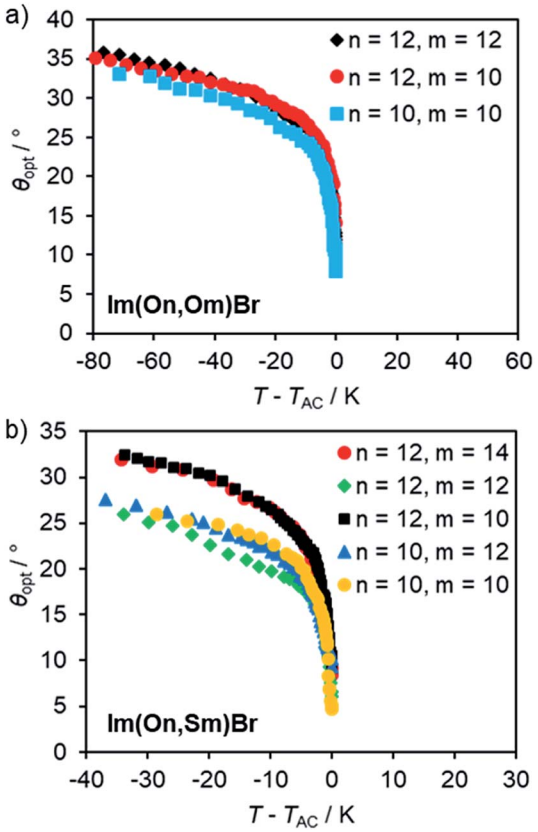

Fig. 14 Optical tilt angle θ_{opt} *vs.* reduced temperature $T - T_{AC}$ for (a) **Im(On,Om)Br** and (b) **Im(On,Sm)Br**. For $\theta_{opt}(T)$ profiles fitted to the power law according to ref. 103 see Fig. S25, ESI.†

Table 2 Maximum layer contraction S_{max}, reduction factor R and optical tilt angle θ_{opt} of ILCs **Im(On,Ym)Br** at the temperature of the maximum layer contraction $T - T_{AC}$

Compound	$T - ;T_{AC}$/K	d_{AC}/Å	d_C/Å	S_{max}/%	θ_{opt}/°	R
Im(O10,O10)Br	−28	64.7	63.4	1.9	28	0.40
Im(O12,O10)Br	−25	66.7	65.9	1.2	30	0.30
Im(O12,O12)Br	−22	72.0	71.4	0.9	29	0.26
Im(O10,S10)Br	−13	68.9	68.1	1.1	24	0.35
Im(O10,S12)Br	−14	72.1	71.4	0.9	23	0.33
Im(O12,S10)Br	−25	71.1	70.4	1.0	31	0.26
Im(O12,S12)Br	−6	74.5	73.8	0.9	19	0.41
Im(O12,S14)Br	−10	76.8	76.5	0.4	27	0.20

Table 3 Layer distance d of imidazolium bromides **Im(On,Ym)Br** and coefficients a_1, a_2, a_3

	T/°C	d_{001}/Å	d_{002}/Å	d_{003}/Å	a_1	a_2	a_3
Im(O12,O10)Br	167	66.7	33.3	22.1	1	0.31	0.52
Im(O12,S10)Br	160	67.7	33.8	22.4	1	0.32	0.60
Im(O12,O12)Br	176	71.1	35.6	23.5	1	0.29	0.41
Im(O12,S12)Br	164	69.9	34.8	23.1	1	0.38	0.55

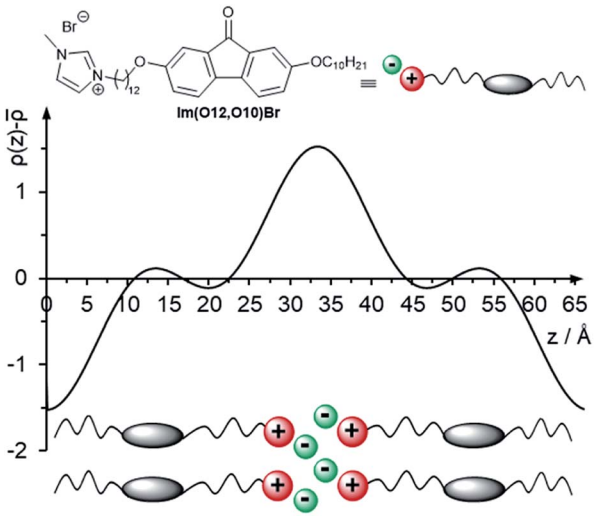

Fig. 15 Electron density profile of **Im(O12,O10)Br** in the SmA phase at 167 °C indicating a bilayer structure and its suggested packing model.

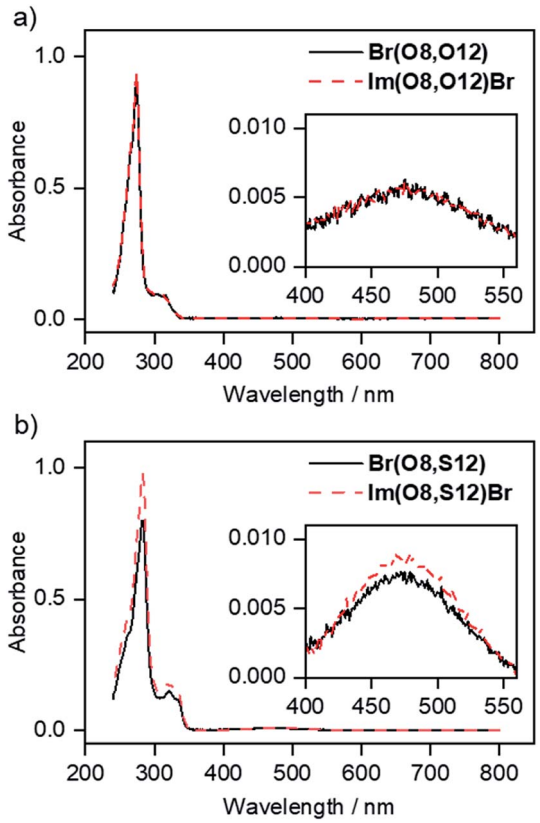

Fig. 16 Absorbance spectra (in $CHCl_3$) of (a) precursor fluorenone **Br(O8,O12)** and ILC **Im(O8,O12)Br** with alkoxy side chains and (b) precursor fluorenone **Br(O8,S12)** and ILC **Im(O8,S12)Br** with thioether side chains. For details of the fluorescence spectra in solution see Fig. S28 and S29 and the corresponding text in the ESI.†

intensity decreased only slightly, but at 60 °C in the SmA phase, the intensity decreased steeply to 20% of the intensity of the isotropic phase. At the SmA–Cr transition again a steep increase

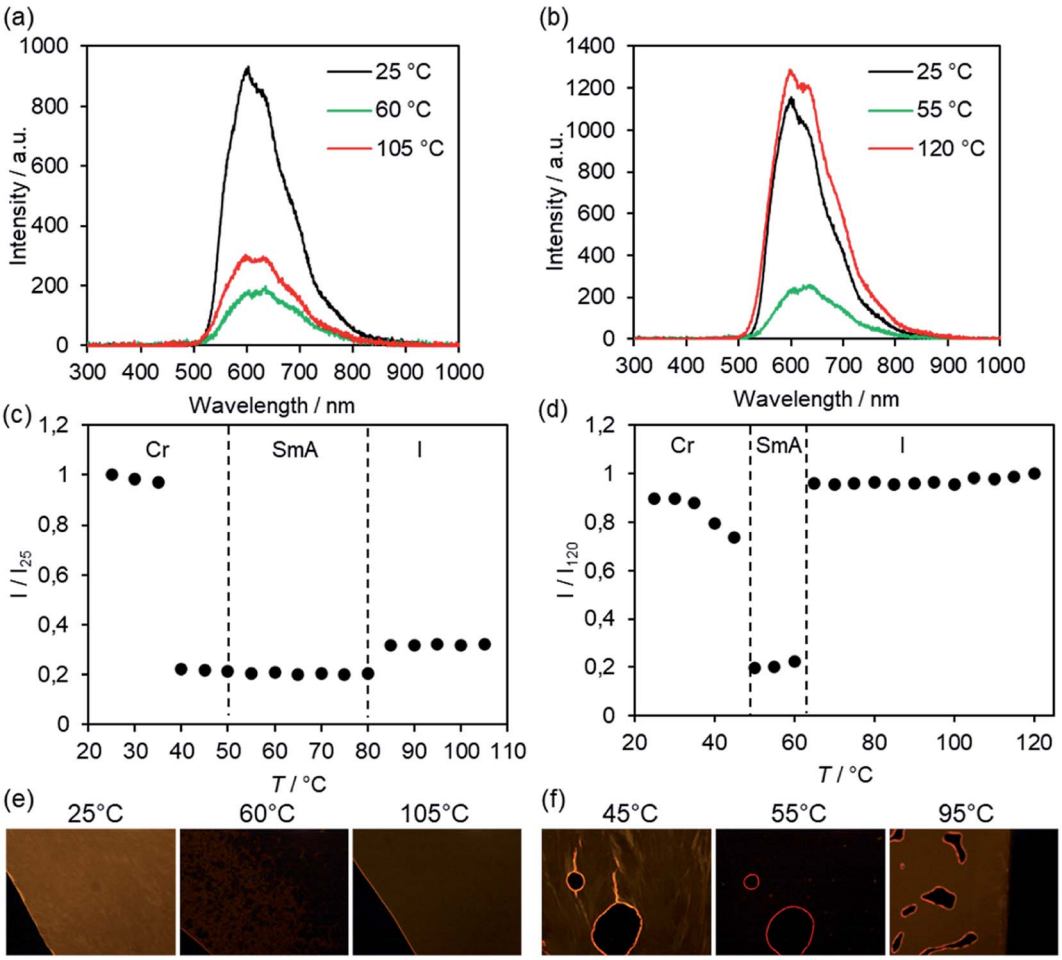

Fig. 17 Emission spectra of (a) **Br(O6,O16)** and (b) **Br(O8,S12)** at different temperatures (λ_{exc} = 350–380 nm). Temperature-dependent emission intensity of (b) **Br(O6,O16)** and (d) **Br(O8,S12)** upon cooling from the isotropic liquid (cooling rate 5 K min^{-1}). Transition temperatures (dashed lines) were determined from the 3rd cooling scan by DSC (Tables S1 and S2, ESI†). POM pictures of (e) **Br(O6,O16)** and (f) **Br(O8,S12)** under irradiation with UV light at the given temperatures, irradiation time 8 s (e) and 4 s (f). POM pictures were taken without analyzer in order to detect sufficient emission intensity.

of the emission was detected, with the intensity being slightly below the emission intensity of the isotropic phase. In other words, the strongest fluorescence was observed at 120 °C. This result is remarkable, because the strongest emission would be expected at low temperature in the highly ordered crystalline phase rather than in the disordered isotropic phase. Presumably, the observed band at 600 nm corresponds to the excimer emission and thus, comparison of ether and thioether derivatives suggests that the interaction between fluorenones in the thioether derivative is more pronounced in the isotropic and crystalline phase as compared to the SmA phase.[126]

The bulk emission behaviour of fluorenone imidazolium triflate **Im(O6,O8)OTf** resembled that of **Br(O6,O16)**. Upon heating of the crystalline phase the emission intensity decreased slightly, but decreased steeply at 80 °C at the Cr–SmA transition to a 10 times lower intensity than that in the Cr phase and remained constant upon further heating and did not increase upon isotropic clearing (Fig. S30, ESI†).

Conclusion

We developed a synthetic strategy to a series of ILCs **ImR(On,Ym)X** consisting of a SmC-promoting central fluorenone core with one alkoxy or thioether side chain and a flexible spacer connected to a SmA-promoting imidazolium head group. Precursor fluorenone bromides **Br(On,Ym)** formed only SmA mesophases, while the fluorenone ILCs **Im(On,Om)Br** carrying an alkoxy side chain indeed displayed both SmA and SmC mesophases. Thereby spacer lengths $n > 10$ increased the stability of the SmC phase up to phase widths of 53 K. Attempts to overcome the high clearing points of ILCs **Im(On,Om)Br**, being close to the thermal decomposition temperature *via* exchange of the bromides against triflate counterions resulted indeed in decreased clearing temperatures. However, the desired effect was accompanied by the loss of the SmC phase and thus triflate was not further considered in these ILCs. ILCs **ImR(On,Sm)Br** with thioether side chain behaved similarly as compared to the corresponding ether derivatives **Im(On,Om)Br**.

In this series enantiotropic SmC mesophases were observed for the H- and Me-substituted imidazolium group with minimum spacer lengths $n = 10$ (R = H) and $n = 6$ (R = Me), while the ethyl substituent (R = Et) caused monotropic SmC phases upon cooling. Fluorenone ILCs **Im(On,Sm)Br** carrying thioethers displayed broader SmC phases as compared to the corresponding ether derivatives **Im(On,Om)Br**, while the opposite trend was observed for the temperature range of the SmA phase, suggesting that S–S interactions are beneficial for SmC phases in ILCs. Alternatively, the larger sulfur in the thioether side chains might be better accommodated in a tilted than a non-tilted orientation.

POM observations of a color change of the textures during the SmA–SmC phase transition indicated an increase in the birefringence of the SmC phase which is correlated with an increased orientational order as expected for de Vries-like materials.[30,108] In XRD measurements higher order reflections were visible suggesting a high degree of translational order in the smectic phase which may originate from strong nano-segregation of the ionic imidazolium head group.[30] From d/d_{AC} *vs.* $T - T_{AC}$ profiles maximum layer contraction values S_{max} ranging from 0.4 to 2.1% were obtained. The optical tilt angles θ_{opt} measured by POM, and finally the calculation of the reduction factor R based on layer spacings d/d_{AC} and θ_{opt} values gave further evidence for de Vries-like behaviour. The R values of ILCs **ImR(On,Ym)Br** ranged from 0.2 to 0.41 and are comparable to those of known neutral liquid crystalline compounds.[50,53,65] The most promising de Vries ILC was thioether derivative **Im(O12,S14)Br** ($S_{max} = 0.4\%$, $R = 0.20$).

Emission spectra of selected derivatives revealed "off–on" effects because the emission intensity strongly depended on the phase type (crystalline, liquid crystalline, isotropic). For bromides **Br(On,Om)** with an alkoxy side chain, the highest intensity observed in the crystalline state steeply decreased at the Cr–SmA transition and increased in the isotropic liquid. Bromide **Br(O8,S12)** with thioether side chain showed a reverse behaviour, *i.e.* a steep decrease of highest intensity in the isotropic liquid upon SmA transition followed by an increase at the SmA–Cr phase transition. The emission intensity profile of ILC **Im(O6,O8)OTf** resembled that of **Br(On,Om)** with the strongest intensity in the crystalline state. After abrupt reduction at the Cr–SmA transition, however, the intensity remained nearly constant also in the isotropic liquid.

In conclusion, we have demonstrated that the combination of charged imidazolium head groups with calamitic fluorenones carrying a lateral polar group and a flexible tether generates ILCs with remarkably low layer shrinkage during SmA–SmC transition. Moreover, fluorenone ILCs and their precursor bromides possess a strong solid state luminescence, which is switched off in the SmA phase and in case of **Br(O8,S12)** is recovered in the isotropic phase. The emission observed in the solid state is the excimer emission corresponding to the interaction between fluorenone moieties, indicating aggregation-induced emission (AIE) behaviour,[127,128] which is much stronger in the isotropic and crystalline phase than in the SmA phase for **Br(O8,S12)**. The phenomenon is less pronounced for the fully oxygenated compound. Thus, our approach has provided access to novel de Vries as well as thermoluminescent materials.

Conflicts of interest

There are no conflicts to declare.

Acknowledgements

This work was supported by the Deutsche Forschungsgemeinschaft (LA 907/17-1 and LA 907/20-1, project SNAPSTER), the ANR (ANR-18-CE92-0026-01), the Deutsche Akademische Austauschdienst (DAAD Procope project PLISE), Ministère de l'Europe et des Affaires étrangères, Ministère de l'Enseignement supérieur, de la Recherche et de l'Innovation (PHC Procope), the Ministerium für Wissenschaft, Forschung und Kunst des Landes Baden-Württemberg and the Carl-Schneider-Stiftung Aalen (shared instrumentation grant). We would like to thank Prof. Frank Giesselmann for helpful discussions.

References

1 K. Goossens, K. Lava, C. W. Bielawski and K. Binnemans, *Chem. Rev.*, 2016, **116**, 4643–4807.
2 M. Mansueto and S. Laschat, in *Handbook of Liquid Crystals*, ed. J. W. Goodby, P. J. Collings, T. Kato, C. Tschierske, H. Gleeson and P. Raynes, Wiley-VCH, Weinheim, 2nd edn, 2014, vol. 6, pp. 231–280.
3 S. Chen and S. H. Eichhorn, *Isr. J. Chem.*, 2012, **52**, 830–843.
4 K. V. Axenov and S. Laschat, *Materials*, 2011, **4**, 206–259.
5 L. Douce, J.-M. Suisse, D. Guillon and A. Taubert, *Liq. Cryst.*, 2011, **38**, 1653–1661.
6 K. Binnemans, *Chem. Rev.*, 2005, **105**, 4148–4204.
7 V. Causin and G. Saielli, in *Green Solvents II: Properties and Applications of Ionic Liquids*, ed. A. Mohammad and D. Imamuddin, Springer, Dordrecht, 2012, pp. 79–118.
8 S. K. Pal and S. Kumar, in *Biosensors Nanotechnology*, ed. A. Tiwani and A. P. F. Turner, Scrivener Publishing, Berkeley, MA 2014, pp. 267–314.
9 D. Högberg, B. Soberats, R. Yatagai, S. Uchida, M. Yoshio, L. Kloo, H. Segawa and T. Kato, *Chem. Mater.*, 2016, **28**, 6493–6500.
10 R. Atasiei, M. Raicopol, C. Andronescu, A. Hanganu, A. L. Alexe-Ionescu and G. Barbero, *J. Mol. Liq.*, 2018, **267**, 81–88.
11 F. Yuan, S. Chi, S. Dong, X. Zou, S. Lv, L. Bao and J. Wang, *Electrochim. Acta*, 2019, **294**, 249–259.
12 K. Stappert and A.-V. Mudring, *RSC Adv.*, 2015, **5**, 16886–16896.
13 S. Kohmoto, Y. Hara and K. Kishikawa, *Tetrahedron Lett.*, 2010, **51**, 1508–1511.
14 K. Goossens, K. Lava, P. Nockemann, T. Van Hecke, L. Van Meervelt, P. Pattison, K. Binnemans and T. Cardinaels, *Langmuir*, 2009, **25**, 5881–5897.
15 N. Trbojevic, J. C. Haenle, T. Wöhrle, J. Kirres and S. Laschat, *Liq. Cryst.*, 2016, **43**, 1135–1147.

16 G. F. Starkulla, S. Klenk, M. Butschies, S. Tussetschläger and S. Laschat, *J. Mater. Chem.*, 2012, **22**, 21987–21997.
17 N. Kapernaum, E. Wuckert, W. Frey, S. Marino, M. Wahl, F. Giesselmann and S. Laschat, *J. Phys. Org. Chem.*, 2018, **31**, e3779.
18 N. Kapernaum, C. Müller, S. Moors, M. C. Schlick, E. Wuckert, S. Laschat and F. Giesselmann, *ChemPhysChem*, 2016, **17**, 4116–4123.
19 A. Sanchez-Castillo, M. A. Osipov, S. Jagiella, Z. H. Nguyen, M. Kašpar, V. Hamplova, J. Maclennan and F. Giesselmann, *Phys. Rev. E: Stat., Nonlinear, Soft Matter Phys.*, 2012, **85**, 061703.
20 W. Haase, Z. X. Fan and H. J. Müller, *J. Chem. Phys.*, 1988, **89**, 3317–3322.
21 A. J. Leadbetter and E. K. Norris, *Mol. Phys.*, 1979, **38**, 669–686.
22 W. L. McMillan, *Phys. Rev. A: At., Mol., Opt. Phys.*, 1972, **6**, 936–947.
23 N. Kapernaum and F. Giesselmann, *Phys. Rev. E: Stat., Nonlinear, Soft Matter Phys.*, 2008, **78**, 062701.
24 J. Watanabe and M. Hayashi, *Macromolecules*, 1989, **22**, 4083–4088.
25 E. F. Gramsbergen and W. H. De Jeu, *Liq. Cryst.*, 1989, **4**, 449–455.
26 Y. Takanishi, A. Ikeda, H. Takezoe and A. Fukuda, *Phys. Rev. E: Stat., Nonlinear, Soft Matter Phys.*, 1995, **51**, 400–406.
27 D. Nonnenmacher, S. Jagiella, Q. X. Song, R. P. Lemieux and F. Giesselmann, *ChemPhysChem*, 2013, **14**, 2990–2995.
28 M. V. Gorkunov, M. A. Osipov, N. Kapernaum, D. Nonnenmacher and F. Giesselmann, *Phys. Rev. E: Stat., Nonlinear, Soft Matter Phys.*, 2011, **84**, 051704.
29 S. T. Lagerwall, P. Rudquist and F. Giesselmann, *Mol. Cryst. Liq. Cryst.*, 2009, **510**, 148–157.
30 J. P. F. Lagerwall and F. Giesselmann, *ChemPhysChem*, 2006, **7**, 20–45.
31 A. de Vries, *J. Chem. Phys.*, 1979, **71**, 25–31.
32 A. de Vries, *Mol. Cryst. Liq. Cryst.*, 1979, **49**, 179–185.
33 A. de Vries, A. Ekachai and N. Spielberg, *Mol. Cryst. Liq. Cryst.*, 1979, **49**, 143–152.
34 V. Swaminathan, V. P. Panov, A. Panov, D. Rodriguez-Lojo, P. J. Stevenson, E. Gorecka and J. K. Vij, *J. Mater. Chem. C*, 2020, **8**, 4859–4868.
35 N. Yadav, V. Swaminathan, V. P. Panov, R. Dhar and J. K. Vij, *Phys. Rev. E: Stat., Nonlinear, Soft Matter Phys.*, 2019, **100**, 052704.
36 Y. Yamada, W. Sano and A. Fukuda, *Mol. Cryst. Liq. Cryst.*, 2019, **682**, 1–7.
37 A. A. S. Green, M. R. Tuchband, R. Shao, Y. Shen, R. Visvanathan, A. E. Duncan, A. Lehmann, C. Tschierske, E. D. Carlson, E. Guzman, M. Kolber, D. M. Walba, C. S. Park, M. A. Glaser, J. E. Maclennan and N. A. Clark, *Phys. Rev. Lett.*, 2019, **122**, 107801.
38 D. Goswami, P. K. Mandal, O. Gutowski and A. Sarma, *Liq. Cryst.*, 2019, **46**, 2115–2126.
39 S. P. Sreenilayam, D. Rodriguez-Lojo, D. M. Agra-Kooijman, J. K. Vij, V. P. Panov, A. Panov, M. R. Fisch, S. Kumar and P. J. Stevenson, *Phys. Rev. Mater.*, 2018, **2**, 025603.
40 W. M. Zoghaib, C. Carboni, F. A. Kashoub, J. S. Al-Rushidi, B. Y. Al-Jabri, A. S. Al-Alawi and H. F. Al-Mendhry, *Mol. Cryst. Liq. Cryst.*, 2018, **666**, 54–64.
41 V. Swaminathan, V. P. Panov, A. Kocot and J. K. Vij, *J. Chem. Phys.*, 2019, **150**, 084901.
42 V. Swaminathan, V. P. Panov, S. P. Sreenilayam, Y. P. Panarin and J. K. Vij, *Liq. Cryst.*, 2019, **46**, 1246–1251.
43 S. P. Sreenilayam, D. Rodriguez-Lojo, V. P. Panov, V. Swaminathan, J. K. Vij, Y. P. Panarin, E. Gorecka, A. Panov and P. J. Stevenson, *Phys. Rev. E: Stat., Nonlinear, Soft Matter Phys.*, 2017, **96**, 042701.
44 N. Yadav, V. P. Panov, V. Swaminathan, S. P. Sreenilayam, J. K. Vij, T. S. Perova, R. Dhar, A. Panov, D. Rodriguez-Lojo and P. J. Stevenson, *Phys. Rev. E: Stat., Nonlinear, Soft Matter Phys.*, 2017, **95**, 062704.
45 W. H. de Jeu, *Physical Properties of Liquid Crystalline Materials*, Gordon and Breach, New York, 1980.
46 S. Chandrasekhar, *Liquid Crystals*, Cambridge University Press, Cambridge, 2003.
47 P. G. de Gennes, *The Physics of Liquid Crystals*, Clarendon Press, Oxford, 1975.
48 Z. Ahmed, C. Müller, J. J. Johnston, K. Nguyen, C. P. J. Schubert, K. Abitaev, S. Marino, F. Giesselmann and R. P. Lemieux, *Liq. Cryst.*, 2019, **46**, 896–904.
49 C. Müller, C. P. J. Schubert, R. P. Lemieux and F. Giesselmann, *ChemPhysChem*, 2018, **19**, 2703–2708.
50 C. P. J. Schubert, C. Müller, A. Bogner, F. Giesselmann and R. P. Lemieux, *Soft Matter*, 2017, **13**, 3307–3313.
51 C. P. J. Schubert, C. Müller, F. Giesselmann and R. P. Lemieux, *J. Mater. Chem. C*, 2016, **4**, 8483–8489.
52 C. P. J. Schubert, C. Müller, M. D. Wand, F. Giesselmann and R. P. Lemieux, *Chem. Commun.*, 2015, **51**, 12601–12604.
53 C. P. J. Schubert, A. Bogner, J. H. Porada, K. Ayub, T. Andrea, F. Giesselmann and R. P. Lemieux, *J. Mater. Chem. C*, 2014, **2**, 4581–4589.
54 Q. Song, D. Nonnenmacher, F. Giesselmann and R. P. Lemieux, *J. Mater. Chem. C*, 2013, **1**, 343–350.
55 J. C. Roberts, N. Kapernaum, F. Giesselmann and R. P. Lemieux, *J. Am. Chem. Soc.*, 2008, **130**, 13842–13843.
56 L. Li, C. D. Jones, J. Magolan and R. P. Lemieux, *J. Mater. Chem.*, 2007, **17**, 2313–2318.
57 M. Thompson, C. Carkner, A. Bailey, N. J. Mosey, N. Kapernaum and R. P. Lemieux, *Liq. Cryst.*, 2014, **41**, 1246–1260.
58 M. Thompson, C. Carkner, N. J. Mosey, N. Kapernaum and R. P. Lemieux, *Soft Matter*, 2015, **11**, 3860–3868.
59 S. P. Sreenilayam, D. M. Agra-Kooijman, V. P. Panov, V. Swaminathan, J. K. Vij, Y. P. Panarin, A. Kocot, A. Panov, D. Rodriguez-Lojo, P. J. Stevenson, M. R. Fisch and S. Kumar, *Phys. Rev. E: Stat., Nonlinear, Soft Matter Phys.*, 2017, **95**, 032701.
60 W. M. Zoghaib, A. K. George, C. Carboni, M. Surekha, A. V. N. Ashok Kumar, P. V. Chalapathy and D. M. Potukuchi, *Soft Mater.*, 2018, **16**, 166–185.
61 W. M. Zoghaib, C. Carboni, J. Al-Rawahi, F. Al-Rubaiei, H. Al-Bulushi, M. Al-Aufi, M. Al-Harrasi, S. Al-Kalbani and A. Al-Kiyumi, *Mol. Cryst. Liq. Cryst.*, 2016, **632**, 114–123.

62 M. Kohout, A. Bubnov, J. Šturala, V. Novotná and J. Svoboda, *Liq. Cryst.*, 2016, **43**, 1472–1485.
63 W. M. Zoghaib, C. Carboni, H. Al-Hinai, S. Al-Abri, S. Al-Kasbi, E. Al-Nasseri, M. Al-Masroori, M. Al-Yahyaee and S. Al-Busaidi, *Mol. Cryst. Liq. Cryst.*, 2015, **612**, 183–190.
64 G.-Y. Yeap, T.-N. Chan, W.-S. Yam, K. Madrak, D. Pociecha and E. Gorecka, *Liq. Cryst.*, 2012, **39**, 1041–1047.
65 K. M. Mulligan, A. Bogner, Q. Song, C. P. J. Schubert, F. Giesselmann and R. P. Lemieux, *J. Mater. Chem. C*, 2014, **2**, 8270–8276.
66 H. K. Singh, S. K. Singh, R. Nandi, D. S. Shankar Rao, S. K. Prasad, R. K. Singh and B. Singh, *RSC Adv.*, 2016, **6**, 57799–57802.
67 Z. Zhang, S. Kaur, B. Kundu, B. K. Sadashiva and H. F. Gleeson, *J. Mater. Chem. C*, 2017, **5**, 1195–1205.
68 M. Alaasar, M. Prehm, M.-G. Tamba, N. Sebastián, A. Eremin and C. Tschierske, *ChemPhysChem*, 2016, **17**, 278–287.
69 S. H. Ryu, T. J. Shin, T. Gong, Y. Shen, E. Korblova, R. Shao, D. M. Walba, N. A. Clark and D. K. Yoon, *Phys. Rev. E: Stat., Nonlinear, Soft Matter Phys.*, 2014, **89**, 032502.
70 Y. Shen, L. Wang, R. Shao, T. Gong, C. Zhu, H. Yang, J. E. Maclennan, D. M. Walba and N. A. Clark, *Phys. Rev. E: Stat., Nonlinear, Soft Matter Phys.*, 2013, **88**, 062504.
71 D. M. Walba, H. Yang, P. Keller, C. Zhu, R. Shao, D. A. Coleman, C. D. Jones and N. A. Clark, *Macromol. Rapid Commun.*, 2009, **30**, 1894–1899.
72 N. Kapernaum, D. M. Walba, E. Korblova, C. Zhu, C. Jones, Y. Shen, N. A. Clark and F. Giesselmann, *ChemPhysChem*, 2009, **10**, 890–892.
73 D. M. Walba, E. Korblova, L. Eshdat, M. C. Biewer, H. Yang, C. Jones, M. Nakata, M. Talarico, R. Shao and N. A. Clark, *J. Soc. Inf. Disp.*, 2007, **15**, 585–588.
74 J. P. F. Lagerwall, D. Coleman, E. Körblova, C. Jones, R. Shao, J. M. Otón, D. M. Walba, N. Clark and F. Giesselmann, *Liq. Cryst.*, 2006, **33**, 17–23.
75 J. A. McCubbin, X. Tong, Y. Zhao, V. Snieckus and R. P. Lemieux, *Chem. Mater.*, 2005, **17**, 2574–2581.
76 J. A. McCubbin, V. Snieckus and R. P. Lemieux, *Liq. Cryst.*, 2005, **32**, 1195–1203.
77 J. A. McCubbin, X. Tong, R. Wang, Y. Zhao, V. Snieckus and R. P. Lemieux, *J. Am. Chem. Soc.*, 2004, **126**, 1161–1167.
78 K. Takatoh, K. Sunohara and M. Sakamoto, *Mol. Cryst. Liq. Cryst.*, 1988, **164**, 167–178.
79 M. D. Harjung, C. P. J. Schubert, F. Knecht, J. H. Porada, R. P. Lemieux and F. Giesselmann, *J. Mater. Chem. C*, 2017, **5**, 7452–7457.
80 A. V. Ivanov, S. A. Lyakhov, M. Y. Yarkova, A. I. Galatina and A. V. Mazepa, *Russ. J. Gen. Chem.*, 2002, **72**, 1435–1438.
81 R. B. Lemieux, *Acc. Chem. Res.*, 2001, **34**, 845–853.
82 A. Schultz, S. Laschat, A. Saipa, F. Giesselmann, M. Nimtz, J. L. Schulte, A. Baro and B. Miehlich, *Adv. Funct. Mater.*, 2004, **14**, 163–168.
83 Y. Wang, Y. Liu, J. Luo, H. Qi, X. Li, M. Nin, M. Liu, D. Shi, W. Zhu and Y. Cao, *Dalton Trans.*, 2011, **40**, 5046–5051.
84 S. V. Subrahmanyam, P. V. Chelapathi, S. Mahabaleshwara, M. Srinivasulu, A. K. George and D. M. Potukuchi, *Phys. B*, 2014, **450**, 173–184.
85 M.-C. Yeh, Y.-L. Su, M.-C. Tzeng, C. W. Ong, T. Kajitani, H. Enozawa, M. Takata, Y. Koizumi, A. Saeki, S. Seki and T. Fukushima, *Angew. Chem.*, 2013, **125**, 1065–1068; *Angew. Chem. Int. Ed.*, 2013, **52**, 1031–1034.
86 J. R. Epperson, M. A. Bruce, J. D. Catt, J. A. Deskus, D. B. Hodges, G. N. Karageorge, D. J. Keavy, C. D. Mahle, R. J. Mattson, A. A. Ortiz, M. F. Parker, K. S. Takaki, B. T. Watson and J. P. Yevich, *Bioorg. Med. Chem.*, 2004, **12**, 4601–4611.
87 S. R. D. George, T. E. Elton and J. B. Harper, *Org. Biomol. Chem.*, 2015, **13**, 10745–10750.
88 J. Magano, M. H. Chen, J. D. Clark and T. Nussbaumer, *J. Org. Chem.*, 2006, **71**, 7103–7105.
89 J. Chae, *Arch. Pharm. Res.*, 2008, **31**, 305–309.
90 A. Jankowiak, Z. Debska, J. Romański and P. Kaszyński, *J. Sulfur Chem.*, 2012, **33**, 1–7.
91 S. Choi, M. A. Larson, S. H. Hinrichs and P. Narayanasamy, *Bioorg. Med. Chem. Lett.*, 2016, **26**, 1997–1999.
92 M. Butschies, S. Sauer, E. Kessler, H.-U. Siehl, B. Claasen, P. Fischer, W. Frey and S. Laschat, *ChemPhysChem*, 2010, **11**, 3752–3765.
93 J. Mars, B. Hou, H. Weiss, H. Li, O. Konovalov, S. Festersen, B. M. Murphy, U. Rütt, M. Bier and M. Mezger, *Phys. Chem. Chem. Phys.*, 2017, **19**, 26651–26661.
94 Y. Nozaki, K. Yamaguchi, K. Tomida, N. Taniguchi, H. Hara, Y. Takikawa, K. Sadakane, K. Nakamura, T. Konishi and K. Fukao, *J. Phys. Chem. B*, 2016, **120**, 5291–5300.
95 F. Nemoto, M. Kofu and O. Yamamuro, *J. Phys. Chem. B*, 2015, **119**, 5028–5034.
96 K. Nishikawa, in *Ionic Liquids Further UnCOILed*, ed. N. V. Plechkova and K. R. Seddon, Wiley, Hoboken, 2014, pp. 59–85.
97 A. Abate, A. Petrozza, G. Cavallo, G. Lanzani, F. Matteucci, D. W. Bruce, N. Houbenov, P. Metrangolo and G. Resnati, *J. Mater. Chem. A*, 2013, **1**, 6572–6578.
98 T. Niemann, D. Zaitsau, A. Strate, A. Villinger and R. Ludwig, *Sci. Rep.*, 2018, **8**, 1–7.
99 H. Liu and H. Nohira, *Liq. Cryst.*, 1998, **24**, 719–726.
100 V. F. Petrov, V. A. Vinokurov and V. V. Belyaev, *Mol. Cryst. Liq. Cryst.*, 2010, **518**, 40–59.
101 I. Rupar, K. M. Mulligan, J. C. Roberts, D. Nonnenmacher, F. Giesselmann and R. P. Lemieux, *J. Mater. Chem. C*, 2013, **1**, 3729–3735.
102 J. W. Goodby, I. M. Saez, S. J. Cowling, V. Görtz, M. Draper, A. W. Hall, S. Sia, G. Cosquer, S.-E. Lee and E. P. Raynes, *Angew. Chem.*, 2008, **120**, 2794–2828; *Angew. Chem. Int. Ed.*, 2008, **47**, 2754–2787.
103 Q. Song, D. Nonnenmacher, F. Giesselmann and R. P. Lemieux, *Chem. Commun.*, 2011, **47**, 4781–4783.
104 M. M. Neidhardt, M. Wolfrum, S. Beardsworth, T. Wöhrle, W. Frey, A. Baro, C. Stubenrauch, F. Giesselmann and S. Laschat, *Chem.–Eur. J.*, 2016, **22**, 16494–16504.
105 W. Cao, B. Senthilkumar, V. Causin, V. P. Swamy, Y. Wang and G. Saielli, *Soft Matter*, 2020, **16**, 411–420.

106 P. H. J. Kouwer and T. M. Swager, *J. Am. Chem. Soc.*, 2007, **129**, 14042–14052.
107 I. Dierking, *Textures of Liquid Crystals*, Wiley-VCH, Weinheim, 2003.
108 R. G. Horn, *J. Phys.*, 1978, **39**, 105–109.
109 M. D. Hanwell, D. E. Curtis, D. C. Lonie, T. Vandermeersch, E. Zurek and G. R. Hutchison, *J. Cheminf.*, 2012, **4**, 17.
110 A. J. Leadbetter and P. G. Wrighton, *J. Phys., Colloq.*, 1979, **40**, 234–242.
111 T. Wöhrle, R. Gündemir, W. Frey, F. Knecht, A. Köhn and S. Laschat, *Chem.–Eur. J.*, 2017, **23**, 4149–4159.
112 R. Bartolino, J. Doucet and G. Durand, *Ann. Phys.*, 1978, **3**, 389–395.
113 E. N. Keller, E. Nachaliel, D. Davidov and C. Böffel, *Phys. Rev. A: At., Mol., Opt. Phys.*, 1986, **34**, 4363–4369.
114 W. G. Jang, M. A. Glaser, C. S. Park, K. H. Kim, Y. Lansac and N. A. Clark, *Phys. Rev. E: Stat., Nonlinear, Soft Matter Phys.*, 2001, **64**, 051712.
115 D. M. Walba and N. A. Clark, *Proc. SPIE*, 1987, **825**, 81–87.
116 D. M. Walba and N. A. Clark, *Ferroelectrics*, 1988, **84**, 65–72.
117 D. M. Walba, H. A. Razavi, A. Horiuchi, K. F. Eidman, B. Otterholm, R. C. Haltiwanger, N. A. Clark, R. Shao, D. S. Parmar, M. D. Wand and R. T. Vohra, *Ferroelectrics*, 1991, **113**, 21–36.
118 M. D. Radcliffe, M. L. Brostrom, K. A. Epstein, A. G. Rappaport, B. N. Thomas, R. Shao and N. A. Clark, *Liq. Cryst.*, 1999, **26**, 789–794.
119 P. Davidson and L. Strzelecki, *Liq. Cryst.*, 1988, **3**, 1583–1595.
120 S. Aeffner, T. Reusch, B. Weinhausen and T. Salditt, *Eur. Phys. J. E*, 2009, **30**, 205–214.
121 P. Davidson and A. M. Levelut, *Liq. Cryst.*, 1992, **11**, 469–517.
122 F. Xu, H. Wang, X. Du, W. Wang, D.-E. Wang, S. Chen, X. Han, N. Li, M.-S. Yuan and J. Wang, *Dyes Pigm.*, 2016, **129**, 121–128.
123 T.-H. Huang, X.-C. Li, Y.-H. Wang, Z.-H. Kang, R. Lu, E.-L. Miao, F. Wang, G.-W. Wang and H.-Z. Zhang, *Opt. Mater.*, 2013, **35**, 1373–1377.
124 A. Poe, A. Della Pelle, S. Byrnes and S. Thayumanavan, *Chem.–Eur. J.*, 2015, **21**, 7721–7725.
125 S. Sergeyev, W. Pisula and Y. H. Geerts, *Chem. Soc. Rev.*, 2007, **36**, 1902–1929.
126 S. Diring, F. Camerel, B. Donnio, T. Dintzer, S. Toffanin, R. Capelli, M. Muccini and R. Ziessel, *J. Am. Chem. Soc.*, 2009, **131**, 18177–18185.
127 J. Luo, Z. Xie, J. W. Y. Lam, L. Cheng, H. Chen, C. Qiu, H. S. Kwok, X. Zhan, Y. Liu, D. Zhu and B. Z. Tang, *Chem. Commun.*, 2001, 1740–1741.
128 J. Mei, N. L. C. Leung, R. T. K. Kwok, J. W. Y. Lam and B. Z. Tang, *Chem. Rev.*, 2015, **115**, 11718–11940.